STRESS IN A MICROGRAVITY BIOREACTOR

A Thesis
Submitted to
the Temple University Graduate Board

In Partial Fulfillment
of the Requirements for the Degree
MASTER OF SCIENCE IN BIOENGINEERING

---

by
George C. Kramarenko
Diploma Date May 2021

Thesis Approvals:

Peter Lelkes, Advisory Chair, Department of Bioengineering
Yah-el Har-el, Thesis Advisor, Department of Bioengineering
Karin Wang, Thesis Advisor, Department of Bioengineering

ABSTRACT

This project involves the design and development of a cell stretching bioreactor device that can work in conjunction with a Random Positioning Machine (RPM) apparatus. Microgravity environments, such as in space, have been shown to induce alterations in cellular development due to inadequate mechanical loading of biological tissue. Because of this, long-term spaceflight has led to many health concerns, including osteoporosis and muscle atrophy. Space travel is rare and costly, making this research difficult to conduct, however; techniques to simulate microgravity on Earth can be achieved by using a Random Positioning Machine. This device has been a beneficial tool used to study the effect gravity has on cellular growth, yet certain tissues in the body, such as bone and muscle, require mechanical stress, strain, and mechanical loading to develop properly. Because of this, a device that can induce strain on cells while subjected to microgravity conditions is needed to further improve cellular research for space exploration. The constructed bioreactor consists of 3D printed and custom-made components that can induce uniaxial cyclic strain on cells adhered to an elastic membrane. Validation and testing of the device have shown that this bioreactor is suitable for cellular experimentation to work in conjunction with an RPM to deliver a controlled amount of strain while under microgravity conditions.

TABLE OF CONTENTS

LIST OF TABLES

Page

LIST OF FIGURES

Page

CHAPTER 1

1. INTRODUCTION

This project will provide a comparison of *in vitro* cell culturing of bodily tissue using strain in microgravity versus the gravity existing on Earth. The possibility to formulate 3-D differentiated tissue-like assemblies through microgravity cell culturing allows for research in many different fields such as regenerative medicine, toxicology, radiation biology, tumorigenesis, and embryogenesis. The best environment that allows for tissue regeneration is one that promotes cell to cell association while also avoiding the highly detrimental effects of high shear stress expressed on the cells. Microgravity environments, such as in space, have expressed these beneficial qualities and have allowed for increased cell aggregation and proliferation [1]. The problem that arises is that there are many unknowns when it comes to determining the effect of microgravity on cellular tissue, and it has shown that long-term space flight has led to a large number of health concerns including cardiovascular and immune disorders, osteoporosis, muscle atrophy, and the disruption of the biological clock [2].

1.1. Effects of Microgravity on Bone

Unlike some tissue of the body, the cells that comprise bone tissue require forces in the form of mechanical loading in order to maintain the structural skeletal anatomy. Bone is a specialized and mineralized connective tissue that has several key roles including acting as a scaffold for muscle to allow for locomotion, protecting soft tissue and vital organs, and providing the storage of phosphate and calcium ions in the body. Bone extracellular matrix has both organic and inorganic components [3]. The organic matrix is composed of about 90% collagen while the remaining portion makes up non-collagenous

endogenous proteins made by the bone cells [4]. On the other hand, the inorganic component comprises the mineralization aspect of the bone and includes calcium and phosphate in the form of hydroxyapatite crystals [5]. The tissue that makes up bone is composed of several cell types, including osteoblasts, osteoclasts, osteocytes, and bone lining cells. Each of them has their own unique role, which includes bone resorption by osteoclasts and bone lining cells, bone formation by osteoblasts, and bone remodeling through osteocytes [6]. These cells all work together in this cycle in order to allow for the process of normal bone remodeling, through which old bone is replaced with new bone. A lack of normal bone remodeling has been shown to cause an imbalance between the resorption and formation of bone and this has resulted in disease states [3].

Research has shown that bone tissue grown under microgravity conditions has resulted in the excessive resorption of bone tissue followed by inadequate bone formation to cause significant bone loss and a rapid decrease of bone minerals, which can result in osteoporosis [7]. This is caused by the release of calcium from the bone into the bloodstream, leading to bone loss [8]. Astronauts aboard the International Space Station (ISS) begin to experience the effect of bone loss as early as just a few days after being in space. Long-term space flight has resulted in increased bone and calcium loss as up to 20% for extended stays, while on average astronauts experience a bone mass loss of 1-2% each month spent in space [9]. The resultant bone loss from space has been credited to alterations in the processes responsible for bone metabolism [10]. Cell culture experiments under microgravity conditions have shown that certain bone cells have undergone changes in the cytoskeletal structure, which negatively impacts bone cell function. The loss in bone mass and density is due to a lack of mechanical loading as a result of the absence of gravity in

space. Research has shown that observed bone loss is first identified in weight-bearing bones, such as ones that compose the spine, femur, and pelvis as up to a 10% reduction in bone mineral density. The cause of this is diminished osteoblast function, which has called for a reduction in bone formation in microgravity conditions due to the lack of mechanical loading [8].

Over the history of prolonged spaceflight, astronauts have used countermeasures to decrease the significance of bone loss as a result of mechanical unloading in space. Of these preventative measures, diet, exercise regimens, and the use of medication or supplementation have been employed. More recently, the Advanced Resistive Exercise Device (ARED) developed by NASA for the ISS is a device commonly used by astronauts to exercise in order to prevent the deleterious effects of microgravity. This machine is able to simulate free-weight exercises in normal gravity conditions to allow for resistance and endurance conditioning training of all the major muscle groups of the body. Research from the ISS has shown that the use of this device coupled with an adequate energy intake and diet helped to maintain bone mass for long-term space missions [9].

1.2. Simulated Microgravity

Long-term space flight exploration has been scarce and proven to be extremely costly over the course of history. Performing cellular experiments in a microgravity environment can be a costly endeavor and simulating the environment on a macro scale can only be done in the span of minutes using free fall or parabolic flight, which provides insufficient data for providing any long-term viable results. For these reasons, the ability to simulate microgravity through the use of a bioreactor without going to space proves to be a method that can be extremely beneficial for research. This resulted in the production

of bioreactors that can simulate microgravity environments on the microscopic scale. The bioreactors that are popular in microgravity research are the fast-rotating clinostat, rotating wall vessel (RWV), and the random positioning machine (RPM). These bioreactors produce such environments for cell culture by reducing the gravitational effects that influence the cells by manipulating the direction or magnitude of gravity. This can be accomplished by producing forces that counteract the gravitational forces, as seen in the clinostat and the rotating wall vessel, or by changing its spatial orientation, as seen in the random positioning machine [11].

The RWV is a bioreactor has that been developed by NASA and is now available commercially through Synthecon Inc. commercially for purchase. The device is able to simulate microgravity conditions through the use of a slow rotating vessel containing the cell suspended media solution. This works by creating spiral trajectories within the vessel through the combination of the movement direction, settling velocity, and the rotation of fluid adapted to match the viscosity and fluid density of the media, and specific weight of the cells [12]. One negative quality of the RWV is that the motion of the device causes fluid shear stress within the vessel [13], [14]. Excessive amounts of shear stress may also occur with the presence of bubbles forming inside the vessel, which can lead to detrimental experimental results [15]. The other limitation of this device is that in order to function under microgravity conditions, in which the media solution is in a constant free fall, then the cells are prevented from settling due to the constant rotation and are always in suspension [11]. This can be troublesome since certain tissues in the body such as bone or muscle require stress and strain in order to prevent the negative effects under microgravity conditions [2]. For this reason, the RWV may not provide results comparative to studies

conducted in space since astronauts are performing several hours of exercise on a daily basis to allow for mechanical loading of their bones and muscles [12].

On the other hand, the use of the Random Positioning Machine (RPM) bioreactor can allow for this type of simulated microgravity experiment due to the device parameters. The RPM works through the rotation of two independent frames in a randomized movement pattern, allowing for the ability to equalize all gravitational vectors enable an environment that simulates microgravity as an average over time [12]. This allows for the absence of shear stress and directly promotes cell-cell contact and initiation of differentiative cellular signaling via specialized cell adhesion molecules [1]. One major advantage of using this bioreactor is that devices or tissue culture plastic vessels can be attached to the stage of the RPM (Figure 1). This novelty can allow for multiple experiments to be run at once, as well as more alternative conditions for cell culture [16].

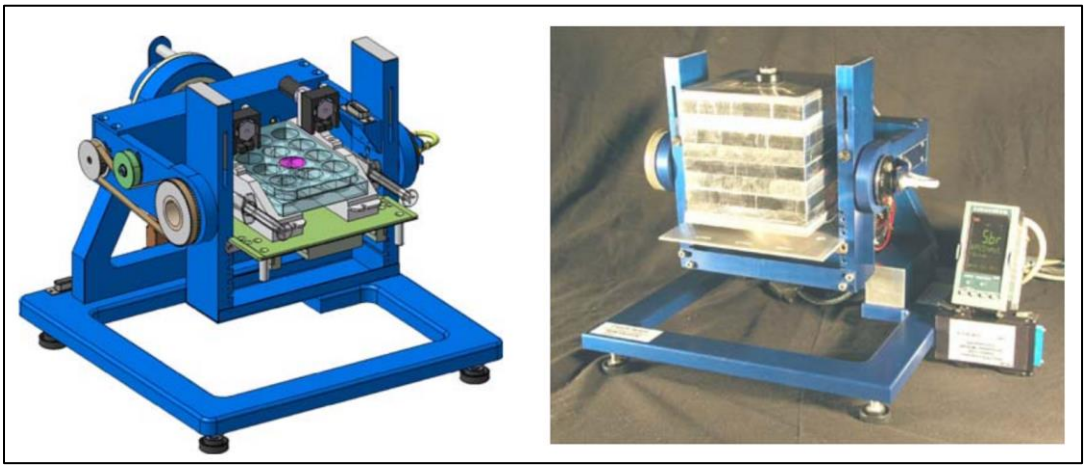

Figure 1. Random Positioning Machine.

A computer-aided design model of the device is shown (Left). Samples can be attached to the stage of the Random Positioning Machine (Right). [16]

1.3. Mechanical Loading Methods

All organisms are mechanosensitive as the conversion to biochemical information from mechanical forces via mechanotransduction is an essential component of structural integrity in cells [17]. As these forces regulate morphogenetic movement needed for the generation of three-dimensional structures [18]. The cardiovascular systems and skeletal structures are good examples of the importance of mechanical forces as the shear stress and pressure from blood flow shaped the morphology and pathology of the heart and vascular system, while gravitational forces and muscular contraction shaped the bones [1]. For these reasons, a disturbance in mechanical forces brought about in a zero and/or partial gravity can lead to adverse health conditions or various diseases. As it has already been described, mechanical loading is a crucial component required for the maintenance of healthy bone cells when subjected to microgravity conditions [19]. Because of this, many studies have been employed to determine how stress and strain applied to these types of cells affect their growth and development. In many cases, performing mechanotransduction experiments *in vivo* has proven to be complex and the results are difficult to quantify. To counteract this result, *in vitro* techniques integrated with *in vivo* stimuli have been developed [20]. In the past, mechanotransduction experiments have been performed with tweezers, micropipettes, and atomic force microscopes (AFM); however, these devices were eventually succeeded by actuators that provided higher efficacy and improvements in data collection [21].

Currently, the most common commercial actuators are the pneumatic, piezoelectric, and the electromotor. The pneumatic actuators utilize either a positive pressure difference, brought about by inflated balloons or negative pressure difference due to vacuum sources (Harshad, 2016) to deform the cellular membrane [22], [23]. Piezoelectric actuators use

nanomanipulation brought about by a piezoelectric motor to induce cell stretching through the conversion of mechanical energy to electrical energy, which is used to determine displacement of strain [24]. Electromotor actuators employ the components that work with its motor to achieve strain on a membrane containing the cells. Each method of actuation carries its share of merits and demerits; for the pneumatic actuators possess a simple and cost-effective setup but lack in precision in comparison to piezoelectric and electromotor actuators. Among the other actuators, piezoelectric demonstrates the highest displacement resolutions, but has the highest manufacturing cost due to the expensive motor system. Additionally, piezoelectric actuators also require direct contact with cells which hinders its performance [21]. Electromotor actuators have shown to have a high degree of precision accompanied by intuitive programming [25].

1.4. Significance of Research

The use of bioreactors to simulate biological processes has been invaluable for research in many different fields. As previously described, several bioreactors have employed methods to simulate microgravity conditions in order to investigate the effects of a lack of mechanical loading on the bone tissue of astronauts on extended spaceflights. These devices have been beneficial tools used to study the effect gravity has on cellular growth, yet certain tissues in the body, such as bone, require mechanical stress, strain, and mechanical loading to develop properly [26]. Additionally, alternative studies have utilized methods to induce mechanical loading on bone cells in order to better understand how applied forces effect cellular growth and development. Taking both of these systems into account, there have been no studies combining the effect of mechanical loading under microgravity conditions on bone health. Because of this, a device that can induce strain on

cells while subjected to microgravity conditions is needed to further improve cellular research for space exploration. Currently in the field, there are devices that can simulate microgravity and there are other devices that can induce strain on cells, yet there is no technology that can do both simultaneously.

This thesis will evaluate the effect of mechanical loading under microgravity conditions on the MC3T3-EI osteoblast cell line, through the use of a custom-made strain device coupled to a random positioning machine. This cell line has acted as the standard model for normal osteoblast differentiation and will be used to understand the effect microgravity has on bone formation [27]. The need for this project is to better determine the effect of microgravity or limited gravity on human cells and tissue for the support of future space exploration, along with the development of replacement organ tissue in the area of tissue engineering. The information that can be attained using a stress inducing bioreactor under microgravity conditions can prove to help better understanding of how cellular activity and function are affected by altering the gravitational force acting upon bone tissue. Research in the field will also allow for the advancement in future space exploration, such as Mars, to determine and predict how the body could potentially react to long-term gravity variations.

CHAPTER 2

2. AIMS OF THE RESEARCH

This thesis seeks to design and develop a novel bioreactor system that is able to apply uniaxial strain to cells under microgravity conditions governed by a Random Positioning Machine. The basis of the research includes the formulation of an elastic membrane material suitable for cellular stretching, the design and construction of a fully functional microgravity bioreactor strain device, and cellular morphological testing using the system. The developed bioreactor can be utilized as a valuable research tool to better understand the effects of mechanical loading on cellular growth and development.

2.1. Specific Aims

Aim 1: Design and formulate an elastic membrane material that is suitable for cyclic uniaxial stretching of cells.

1.1 Analyze membrane design parameters through the use of modelling software in order to justify the capability of continuous uniaxial stretching.

1.2 Investigate the material and mechanical properties of the developed membrane.

Aim 2: Develop a novel bioreactor capable of applying uniaxial strain on cells while subjected to micro/partial gravity conditions governed by a Random Positioning Machine (RPM).

1.1 Design and construct a custom-made bioreactor and demonstrate that the components of the device are leak-proof, sterilizable, and biocompatible.

1.2 Develop a computer-operated, remotely controlled stretching system capable of applying adjustable and a controlled amount of strain on the membrane containing cells, while subjected to the dynamic movement of the RPM.

Aim 3: Use the constructed bioreactor to examine the effect of mechanical loading under reduced gravity conditions using the MC3T3-EI cell-line.

1.1 Evaluate and analyze the effect of strain under reduced gravity in regard to cell alignment, cell shape, and morphology.

Rationale

The intent of this project is to design and develop a novel bioreactor strain device that can work in conjunction with a Random Positioning Machine under reduced gravitational conditions. Currently in the field, there are devices that are able induce strain on cells in a monolayer and there are other devices that can simulate micro or partial gravitational conditions, but there is no device that can do both simultaneously. This project seeks to explore a multifunctional device apparatus that can be utilized for many types of research to determine the effect of mechanical loading in zero or partial gravity. The practical implications of this type of research can be used to better understand the health effects of long-term space flight on astronauts, as well as for future space exploration to Mars.

CHAPTER 3

3. METHODOLOGY

3.1. Aim 1

Polydimethylsiloxane (PDMS) is a silicone elastomer frequently used in microelectromechanical systems due to its various desirable properties [28]. This elastomer is chemically inert, biocompatible, flexible, durable, and inexpensive to produce [29]. Due to these properties, it has been a common substrate selection among bioreactors applying mechanical stress to cells [30]. This aim illustrates the design and formulation of a custom made PDMS membrane aimed specifically for inducing strain on cells. A PDMS membrane has been formulated and tested under cyclic uniaxial strain at varying amounts.

3.1.1. PDMS Membrane Design

Several design parameters were put into place when designing the PDMS membrane to be used as the stretching substrate. When designing the membrane, the American Society for Testing and Materials Standard Test Methods for Vulcanized Rubber and Thermoplastic Elastomers (ASTM D412-16) was used as a reference [31] (Figure 2). Much research has been conducted on the mechanical properties of PDMS according to this ASTM standard, therefore key ratios were utilized in the design to ensure that the sample would have a similar mechanical behavior. The gauge length to gauge width ratio for the ASTM standard is 5.5:1 with a thickness of 3mm, and as a result the designed membrane followed these constraints (Figure 3). Another important feature in the design is the addition of filets on the edges of the PDMS membrane. The purpose of this is to alleviate the high stress at the dynamic and static ends, as well as the slot inserts.

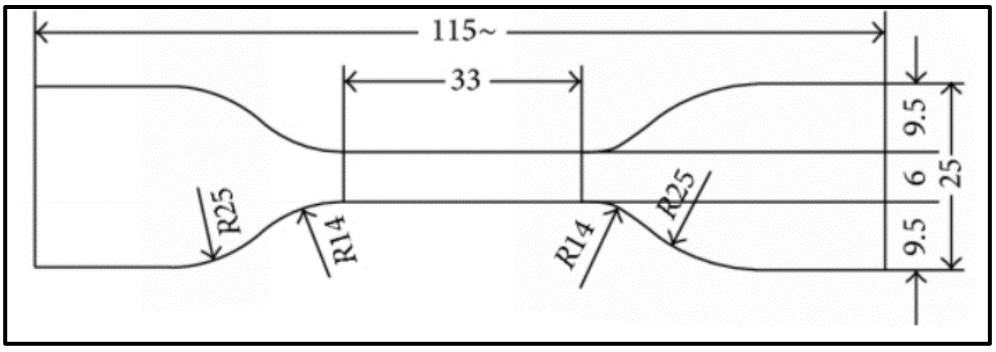

Figure 2. ASTM 412C Standard for Elastomers.

This schematic illustrates the dimensions of the standard tensile test sample utilized according to the American Society for Testing and Materials Standard Test Methods for Vulcanized Rubber and Thermoplastic Elastomers. [31]

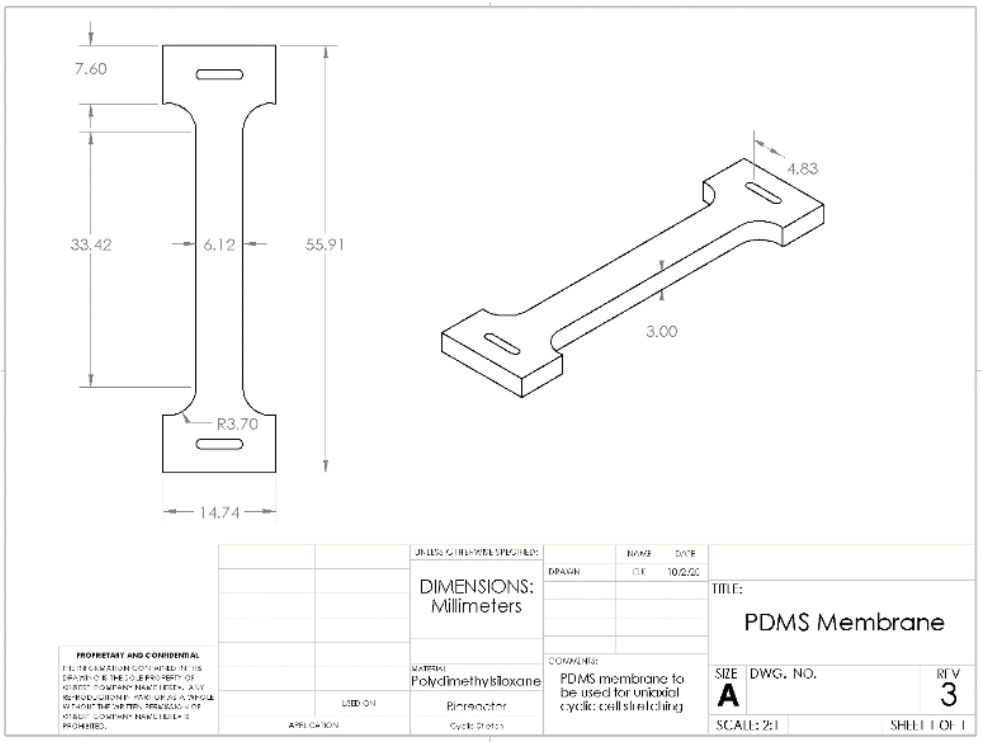

Figure 3. Custom-made PDMS Membrane Design and Dimensions.

This design follows the length to width ratio according to ASTM 412C standard for elastomers.

3.1.2. Modelling Software Analysis

To validate the design of the membrane, mechanical modelling was employed to determine how the substrate would react under applied load. To do this, SolidWorks was utilized to run simulations of the material behavior. The PDMS membrane is designed to have one static fixed end, while the opposing side is the end that the load is applied to dynamically stretch the membrane (Figure 4). In the model, the membrane is fixed at one end at the slot position and the force load is applied to the opposing slot, causing tensile stress along the center axis of the substrate. For this model, a non-linear model was utilized to prescribe a displacement of 2.5 mm. This was done by making the static end a fix face while an advanced fixture called described displacement on the dynamic end using the on rectangular faces setting since this is the geometry of the end. A custom material was created to account for the mechanical properties of PDMS and this information was dictated from the stress-strain literature up to a maximum of 200 points [26]. After this, the material model was altered to make this follow the hyperelastic Blatz Ko model type. Additionally, the solver was adjusted in the study properties tab to direct sparse in order to calculate the computation without data overload. The final step before running the simulation is to create a curvature-based mesh on the membrane which allows for a more accurate analysis since it is able to account for the complicated geometries of the drawing such as fillets and slots. This mesh allows for more focal points on the surface of the membrane and thus yields a more accurate analysis in regard to stress, strain, and displacement along the gauge length.

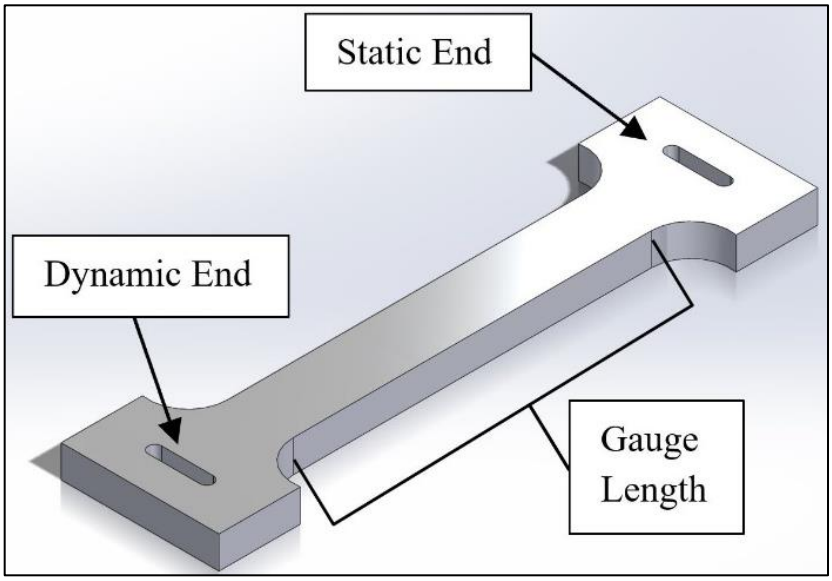

Figure 4. PDMS Membrane Design Layout.

Key features of the designed membrane are illustrated including the gauge area, and both the static and dynamic ends.

3.1.3. PDMS Membrane Formulation

Once working models were developed, the next step was to formulate membrane samples for testing procedures. The most popular form of PDMS is manufactured by Dow Corning and is called Sylgard 184. To produce the PDMS two primary chemicals were needed: Sylgard 184 Elastomer Base and Sylgard 184 Silicone Elastomer Curing agent. The protocol for PDMS formulation used for all studies was performed by measuring out Sylgard 184 Elastomer Base and Sylgard 184 Silicone Elastomer Curing agent into a sterile container to acquire a mass ratio of 10:1 for the base to curing agent. These components were mixed by hand for 10 minutes using a stirring unit [32]. Next, the container with the mixture is placed into a vacuum desiccator in order to remove air bubbles that were caused from the stirring process, and it is kept inside the desiccator for 45 minutes. Once all bubbles are eliminated, the container is removed from the vacuum and a micropipette is

used to transfer 1.408 mL to the mold, which corresponds to the total volume of the designed membrane. The mold is placed into the vacuum desiccator for 30 minutes to remove any newly formed bubbles from the transfer process. After this, the mold is removed from the desiccator and placed inside an oven for 35 minutes at 100℃. This will enable the specimens to fully cure under these conditions. Lastly, remove the cured PDMS from the oven and allow 24 hours of cooling before removing specimens from the mold using a scalpel (Figure 5) [31].

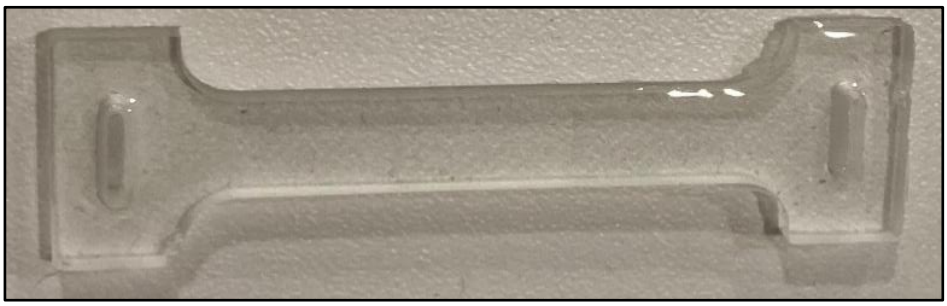

Figure 5. Formulated PDMS Membrane.

The PDMS membrane was made using a base to crosslinker ratio of 10:1 and the curing conditions of 100℃ for 35 minutes.

In order to make consistent and well-defined PDMS samples, a custom-made mold was designed and formulated using 3D printing (Figure 6). Several materials were initially examined as the mold material (Figure 7). When selecting a mold material, it is important to select one that would have a heat deflection temperature above the curing temperature of 100℃ to prevent the melting of the mold and potentially any leachable agents of entering into the PDMS.

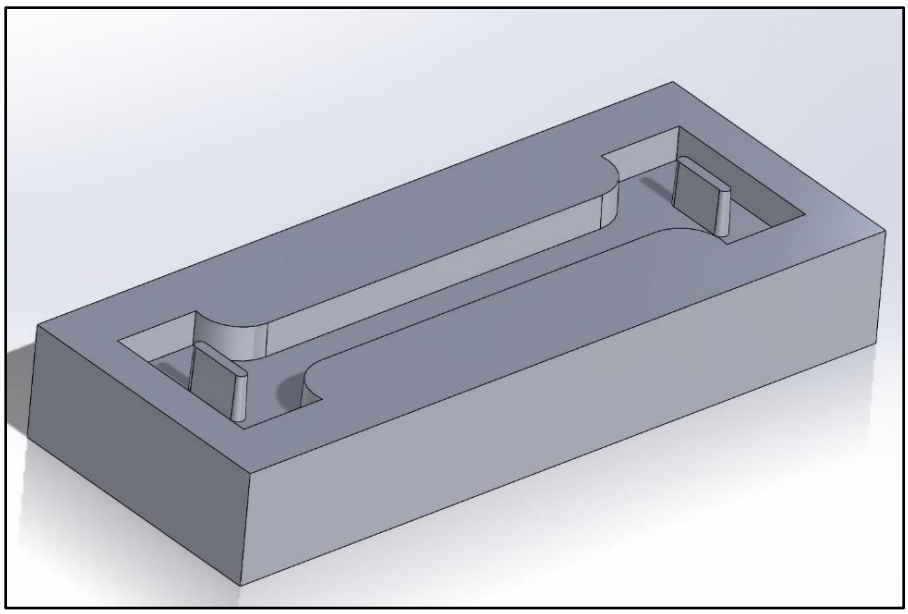

Figure 6. PDMS Membrane Mold.

The mold was designed in SolidWorks and was based off the PDMS membrane dimensions.

PDMS samples were formulated in molds made from a 3D printed material called Onyx and this filament is produced by Markforged. This selection was made since this material exhibits a high heat deflection temperature of 145℃ which allows it to be cured at the desired temperature [33]. This material also has a very fine print resolution which enables the mold to have very accurate specifications and a tight print pattern, while it is also relatively hydrophobic, and this is suitable for curing PDMS. The material is composed of a proprietary blend of nylon and carbon fiber and it take on a black color in appearance (Figure 7). When printing the mold, the infill and top/bottom layers was set to its maximum value.

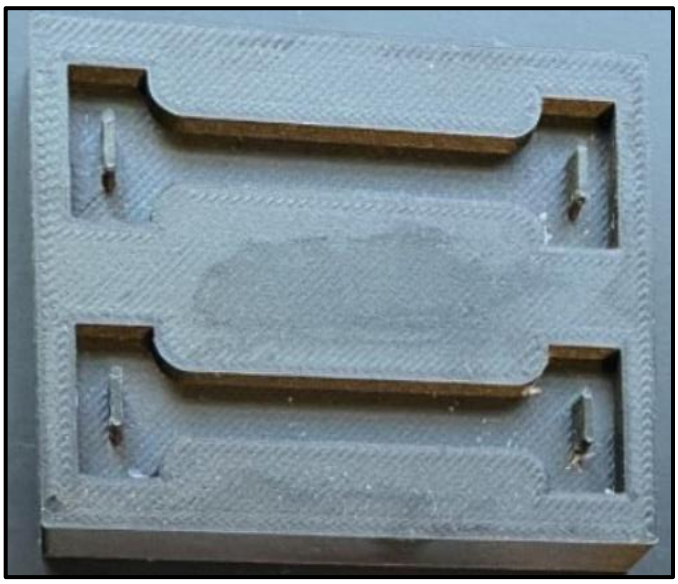

Figure 7. 3D Printed PDMS Membrane Mold.

The mold was printed out of Onyx print filament using the Markforged 3D printer.

3.1.4. PDMS Tensile Test

Once it was proven that successful PDMS membrane could be formulated, the mechanical properties could then be evaluated. An ASTM 412C Elastomer Tensile Test was conducted to assess the Young's Modulus of the elastomer. A new mold was designed based off the ASTM standard and was developed using previous methods (Figure 8) [29]. Tensile test samples were produced using the new mold and the PDMS formulation was held consistent as before (Figure 9). Three specimens were prepared for the tensile assay. The device used for the experiment was an Instron Mini 55 Tensile Tester equipped with Bluehill Universal software (Figure 10).

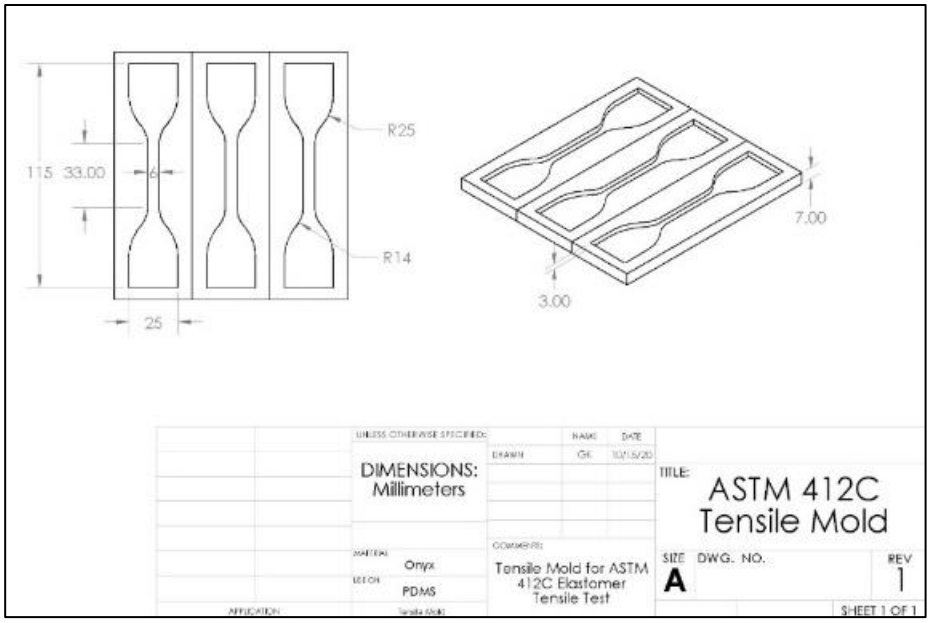

Figure 8. Tensile Test Standard Mold Design.

Schematic based off the ASTM 412C standard for elastomers.

Figure 9. 3D Printed PDMS Tensile Test Mold.

ASTM 412C tensile test mold printed out of Onyx using the Markforged 3D printer.

The set-up of the system is straightforward, and it involved programming the software with the design parameters of the ASTM 412C tensile standard and loading the samples. The test was conducted at a rate of 50 mm/min and data was extracted from the software to indicate position and force for the duration of the test.

Figure 10. ASTM 412C Standard Elastomer Tensile Test Set-up.

Instron Mini 55 Tensile Tester was used to conduct tensile tests on PDMS samples at a rate of 50 mm/min.

3.1.5. PDMS Strain Characterization

Through the use of mechanical modelling and experimental tensile testing procedures, a good understanding was able to be drawn pertaining to the elastic nature of the PDMS samples. However, to further validate the mechanical properties of the membrane a strain characterization assay was performed to identify the engineering strain exhibited on the gauge area of the custom-made PDMS membranes. Five identical membrane samples were formulated, and measurements were taken to ensure the accuracy and consistency of the specimens. Two identical markers were place along the gauge length of the membrane spaced 10 mm apart (Figure 11). This distance was selected because, according to the displacement model, the area within this space experienced uniform tensile stress and strain.

Figure 11. Strain Characterization Set-up.

Two identical markers in green were placed 10 mm apart along the gauge length of the PDMS membrane.

The samples were placed inside the custom-made bioreactor system for testing, fixed at the static end and attached to the actuator to induce dynamic stretching. A video apparatus was used consisting of an overhead tripod to capture quality videos of the system stretching the PDMS membranes.

According to calculations done by the coding system used to power the actuator, the amount of strain could be determined and estimated. For this assay, the value of 5% strain was selected as the strain of choice since this value was indicated as the approximate maximum strain occurring on the membrane given a 2.5 mm displacement. This would then ensure that the system could properly induce the selected amount of strain on the membrane while also providing and validating the PDMS under cyclic stretch to determine the strain characterization under loading conditions. Small video segments were taken for each sample and were analyzed using video tracking software packages including the Tracker Video Analysis and Software Tool [34].

In the video software, samples were marked and tracked during the progression of applied displacement of the actuator to determine the amount of engineering strain being exhibited across the central region of the gauge length define across 10 mm (Figure 12). To evaluate the consistency of the cyclic stretching, each of the samples were analyzed during 5 separate elongation and retraction cycles, then averaged to obtain the value of strain during the cycle.

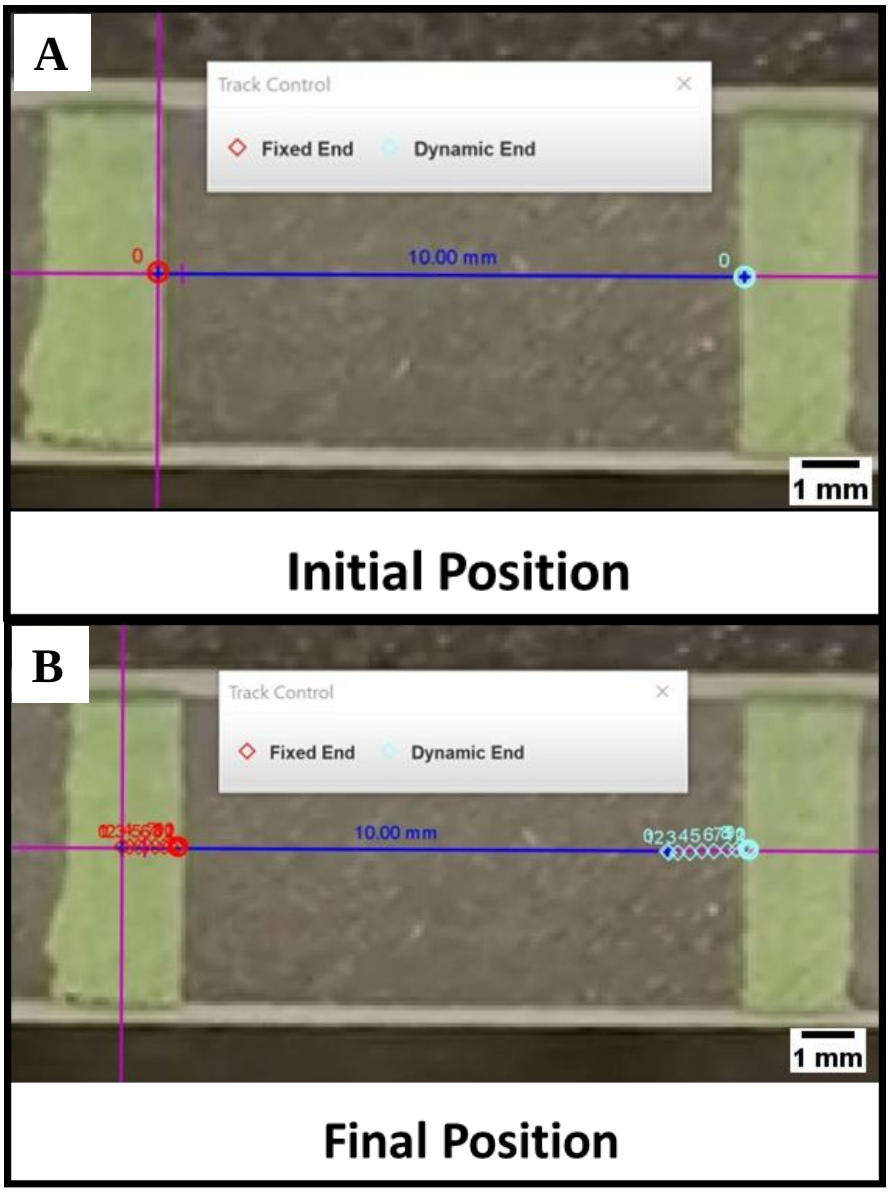

Figure 12. Strain Tracking Characterization Experimentation.

Cyclic uniaxial stretching was performed for five complete cycles. The displacement of the membrane was broken down into steps for both the fixed end (red) and the dynamic end (blue). (A) Initial position of the membrane. (B) Maximum position tracked with step points of strain progression.

3.1.6. Fatigue Testing

The mechanical properties of the PDMS membrane have shown to act as an effective substrate to induce the desired amount of strain while showcasing the ability to elastically load and unload without exhibiting deformation. In the literature, there is a lack of data illustrating mechanical cyclic fatigue loading of silicone-based substrates, therefore a fatigue loading assay is of great interest. Three samples of PDMS were utilized for this assay each containing markings 10 mm apart across the gauge length area were measured before and after stretching to determine if any deformation had occurred. Images of the samples were captured under the Olympus CKX53 microscope to evaluate the structure before and after fatigue loading. Each sample was subjected to 72 hours of cyclic loading at 5% strain across the center of the gauge area.

3.2. Aim 2

This aim will focus on the design and construction of the bioreactor and focus on the application of applying strain to cells. The goal of this aim is to develop a custom-made bioreactor device that is able to apply uniaxial cyclic strain on a PDMS membrane containing adhered cells, which can be operated onto a random positioning machine to perform under microgravity conditions. Inside of a custom-made 3D printed cell culture flask, cells will be adhered to a silicone elastomer membrane that is fixed at one end and attached to a motor shaft to be dynamically stretched on the other end. A linear servo motor will be attached to the motor shaft and will stretch the membrane, which is controlled through a microcomputer system. The entire system will be attached to a custom-made housing unit which will be fixed to the stage of the RPM.

3.2.1. Cell Culture Flask Design

The most crucial component of the bioreactor is the area where the cyclic stretching of cells will take place, therefore a cell culture flask has been formulated to run the experiments (Figure 13).

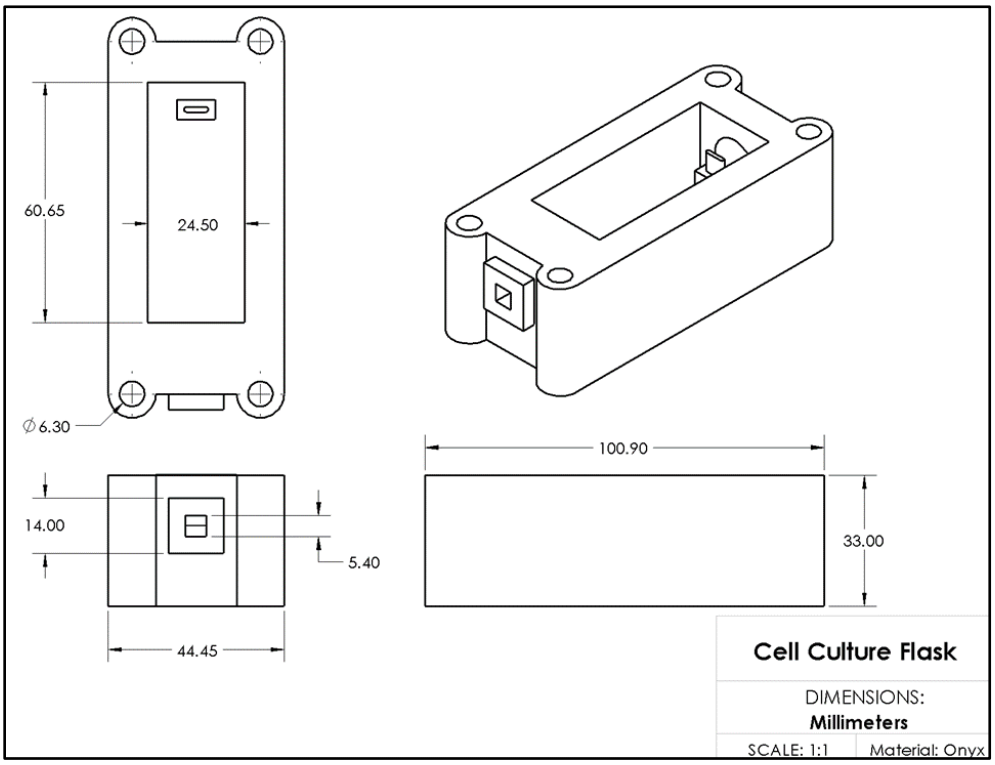

Figure 13. Cell Culture Flask Dimensions.

Schematic illustrates the viewpoints of the designed flask.

The design of the cell culture flask has several key components (Figure 14). It includes an insert shaft entry site which will connect a motor shaft to the PDMS membrane on one side while the other side of the membrane is attached onto a fixed end. Another key feature includes a lid with a built-in viewing platform and an O-ring groove to ensure sealing of the flask to prevent leaking of culture medium solution.

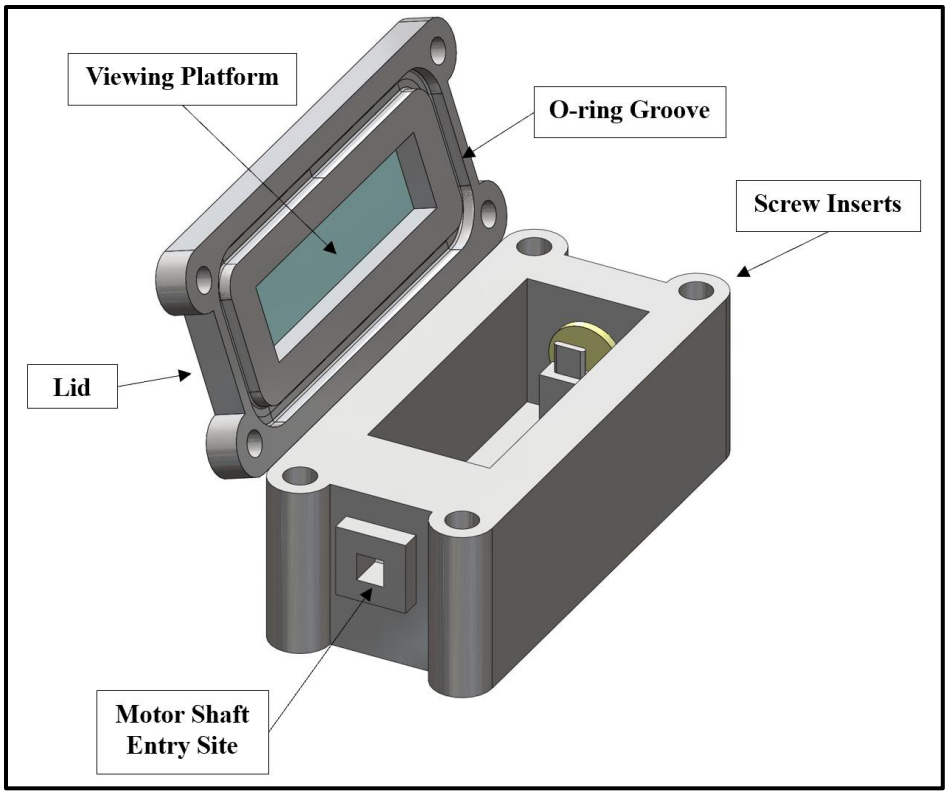

Figure 14. Cell Culture Flask CAD Design.

This cell culture flask was designed with several key features including a lid with a viewing platform, O-ring groove, screw inserts, and a motor shaft entry site.

The viewing platform was made through the use of a press fit using a glass slide and it was sealed to the lid using PDMS. The flask also includes screw insert sites which allows the lid to securely attach to the base. Another important feature is the vented port which is needed to allow for proper gas exchange of the culture flask, and this is needed for proper cell health (Figure 15). The motor shaft entry site was designed in order to compensate the high-pressure area at the outer side of the flask and the low-pressure area at the inner side of the flask. The design introduces a negative pressure gradient from low to high pressure which would prevent any media from leaking at the shaft entry site.

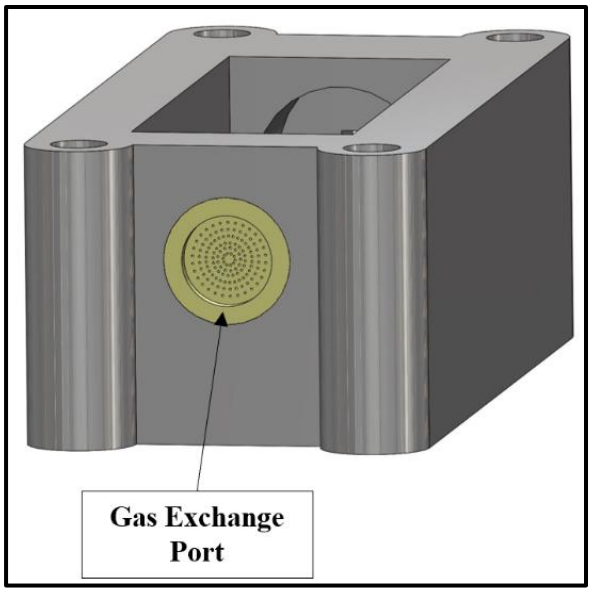

Figure 15. Culture Flask Front View.

Gas exchange port allows proper flask oxygenation.

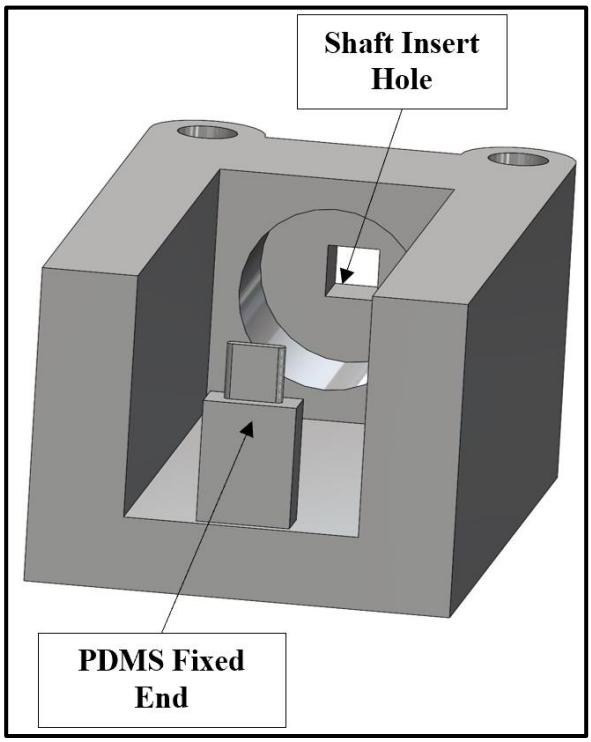

Figure 16. Culture Flask Interior View.

Key features include shaft insert hole and PDMS fixed end.

Aside from the exterior components of the cell culture flask, there are also important interior parts that are essential for cell stretching (Figure 16). Inside the flask, the PDMS fixed end is the site where the static side of the PDMS membrane is attached within the flask, while the shaft insert hole is where the motor shaft enters the flask to attach to the other end of the PDMS membrane to allow for stretching. The insert hole has been designed with a rectangular entry site in order to reduce shaft torsion or rotation from cyclic stretching.

3.2.2. Material Selection & Construction

It is crucial that the culture flask, which will contain the specimen cells must be fully self-contained. This is to prevent the spillage of cell culture medium during the RPM's random motion and the motion of the cell stretching device. The vessel must also be designed to prevent the free flow of the culture medium which will significantly affect experiment results. To prevent the flow of the culture medium from the flask to the ambient surroundings pressure must be considered at all points in the system. Additionally, the device is required to allow the diffusion of air into the flask which is an indispensable component of cell growth. Therefore, the flask must allow for air to enter the flask while simultaneously keeping the culture medium within its control volume.

To account for the complicated geometries of the flask design, 3D printing technology had to be employed for construction. The selection of the proper printing material is of great importance. The interior makeup of the culture flask will be in constant contact with culture media which is providing nutrition for cellular growth. The selected material therefore must be chemically resistive and non-toxic in order to make sure it is safe for cell growth. The material must also have extremely high strength, durability, heat

resistance, and hydrophobicity in order to withstand prolonged durations of time under dynamic and volume filled conditions.

Since this culture flask is suited as a functional prototype, the type and quality of the printing capabilities must be extremely accurate. The material must be able to be printed using a maximum infill and maximum top/bottom layers to guarantee that it can fully contain liquid solutions without it slowly leaching through the material. For all of these reasons, the material selected was Onyx and this was printed on the Markforged 3D printer. Onyx is a custom-made trademark material made out of micro carbon fiber filled nylon. It is printed with exceptional surface finish and has great overall strength, toughness, and chemical resistance. To test these claims, a series of leak test assays were performed on the material (Figure 17).

For this test, a small block was designed to replicate the design parameters of the cell culture flask. The smallest wall thickness on the cell culture flask is 7mm so when designing this test block the thickness was set at this value for all sides.

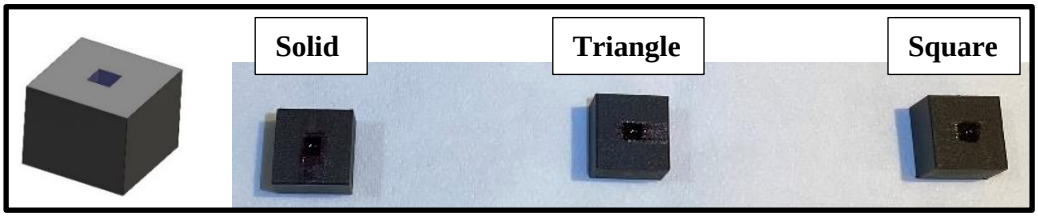

Figure 17. Onyx Test Block Leak Testing.

CAD Drawing (left) and Leak Test Samples (right). The printing parameters were compared using solid, triangular, or square extrusion patterns.

It was also of interest to see if the printing parameters would affect how well the material is able to seal out solutions. Because of this, three blocks were printed with direction infill and layer orientations. The first block was printed with maximum solid infill and maximum top/bottom layers, the second was printed with a triangular infill and set to 75% for both infill and top/bottom layers, and the third block was printed with a square infill set to 75% for both the infill and top/bottom layers.

The test blocks were filled with water containing dye to color the water red so that any leakage would be shown through the color. This was tested by adding in the maximum volume that each block could hold and then waiting to see how much the liquid decreased by over time. This was tested against a control group of tissue culture plastic (TCP) where the same amount of liquid volume was placed onto a petri dish to see how long it would take for evaporation to occur. The solid infill set to the maximum for both print settings showed the best results, yet the solution was still penetrating through the material. In order to combat this, a hydrophilic coating called RainX was used prior to running the test again and this had a drastic effect. The combination of the solid infill to the maximum and the RainX coating yielded the same response as the control group of TCP. This indicated that the solid infill maximum in conjunction with the biocompatible RainX is a viable option to prevent medium from leaking through the material (Table 1).

	Time Taken Until Solution was no Longer Present
Solid	2 hours
Triangle	1 hour
Square	30 minutes
Solid + RainX	6 hours
Triangle + RainX	6 hours
Square + RainX	6 hours
TCP	6 hours

Table 1. Leak Test Results of Onyx Test Material Blocks.

The Onyx print material was tested for its ability to contain solution with and without the use of a RainX coating.

Now that it was proven that the Onyx material could successfully prevent liquid from diffusing through, the material could then be validated for sterilization purposes. Most TCP comes in a sterile environment to protect against contamination and can be sprayed with an alcohol-based solution for sanitization purposes, yet due to the complexity of how the part is made and the nature of the cell stretching system then this had to be sterilized in a different manner compared to other culture flasks. The material properties of Onyx include a high tensile modulus of 1.4 GPa and a heat deflection temperature of 145°C. Given these properties, the material composition would be able to withstand the conditions of an autoclave for sterilization. In order to test this, the same test blocks were utilized from the leak testing [33]. The blocks were measured for their exterior dimensions before

subjecting them to the autoclave and they were run through the machine 5 times on the pipette tip setting, where the dimensions were taken after each time. The dimensions of all three blocks remained the same as the original value after each time of sterilization. This indicated that the material properties of Onyx were optimum for withstanding high temperature and pressure conditions, and that using the autoclave as a method of sterilization is viable. As a result of this, the cell culture flask was printed using the Onyx material with a maximum solid infill and maximum top/bottom layers (Figure 18).

Figure 18. Custom-made Cell Culture Flask.

The culture flask constructed out of the Onyx 3D print material put together with all of its corresponding components.

Leak testing was also performed using the culture flask to verify the results from the block assay. The culture flask was sealed with a plug at the shaft insert and also at the gas exchange areas on the sides of the flask through the use of Tegaderm™. The RainX coated flask was filled with color dyed red water to its maximum volume and placed on top of white paper to signify any leaking of the flask. The flask was filled with this solution for a total of 5 days and the result showed no leaking or permeation through the culture flask. These results illustrated that this material would be suitable to act as a cell culture flask. In order to further prevent leaking, a fine coating of PDMS was added to the walls of the culture flask.

3.2.3. Motor Shaft Design

As previously described, the motor shaft will be the component responsible for the cyclic displacement of the PDMS membrane (Figure 19). It has been designed with an attachment post for the dynamic end of the PDMS membrane to be fixed onto it (Figure 20). In order to prevent leakages from the culture flask due to dynamic motion, an O-ring has been implemented around the head of the motor shaft. The O-ring is designed for dynamic sealing purposes and for this reason it will not tear as readily due to the force of friction during the cyclic motion of stretch. In previous designs the rod of the shaft has been cylindrical, yet a recurring issue was that during certain times this geometry would allow the shaft to rotate and cause a torsional force on the sample which is undesirable. Because of this, a rectangular rod design has been implemented and this has eliminated the rotating of the shaft. Lastly, the end of the rod has been designed with an insert hole for a screw to expand insert to be press-fitted into. This connection allows for the attachment of the shaft to the actuator to allow for cyclic stretching to occur (Figure 23).

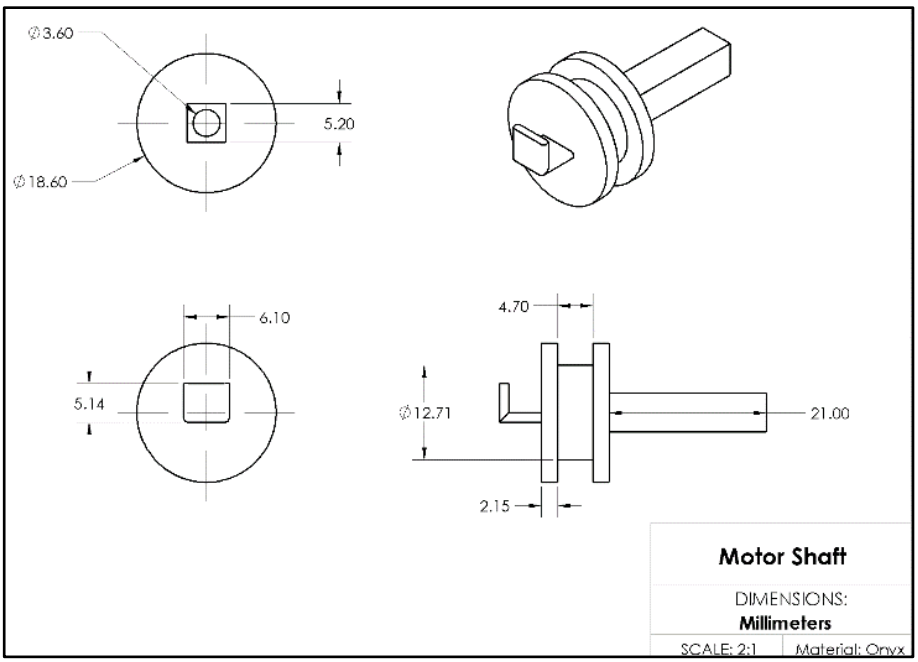

Figure 19. Motor Shaft Drawing Specifications.

Schematic of the motor shaft illustrates the design of the part.

To keep the print material consistent with the culture flask, the motor shaft was also printed out of Onyx. The shaft is a component that will come into contact with the cell culture medium therefore it must be autoclaved for sterilization. From testing the material properties of Onyx, it has proven to be an extremely tough material and able to withstand the conditions of the autoclave. Using this material is also ideal for the shaft application since it has an incredible flexural strength of 81 MPa for a 3D printed material [33]. This is important since there will be a great deal of stress applied on the PDMS attachment post and it is necessary to have material that can withstand cyclic load for long durations of time [34]. Additionally, the flexural modulus of Onyx is 3.6 GPa which is crucial at the post since this is the tendency of a material to resist bending [33]. These mechanical properties ensure that this composite material is a suitable choice for this type of research.

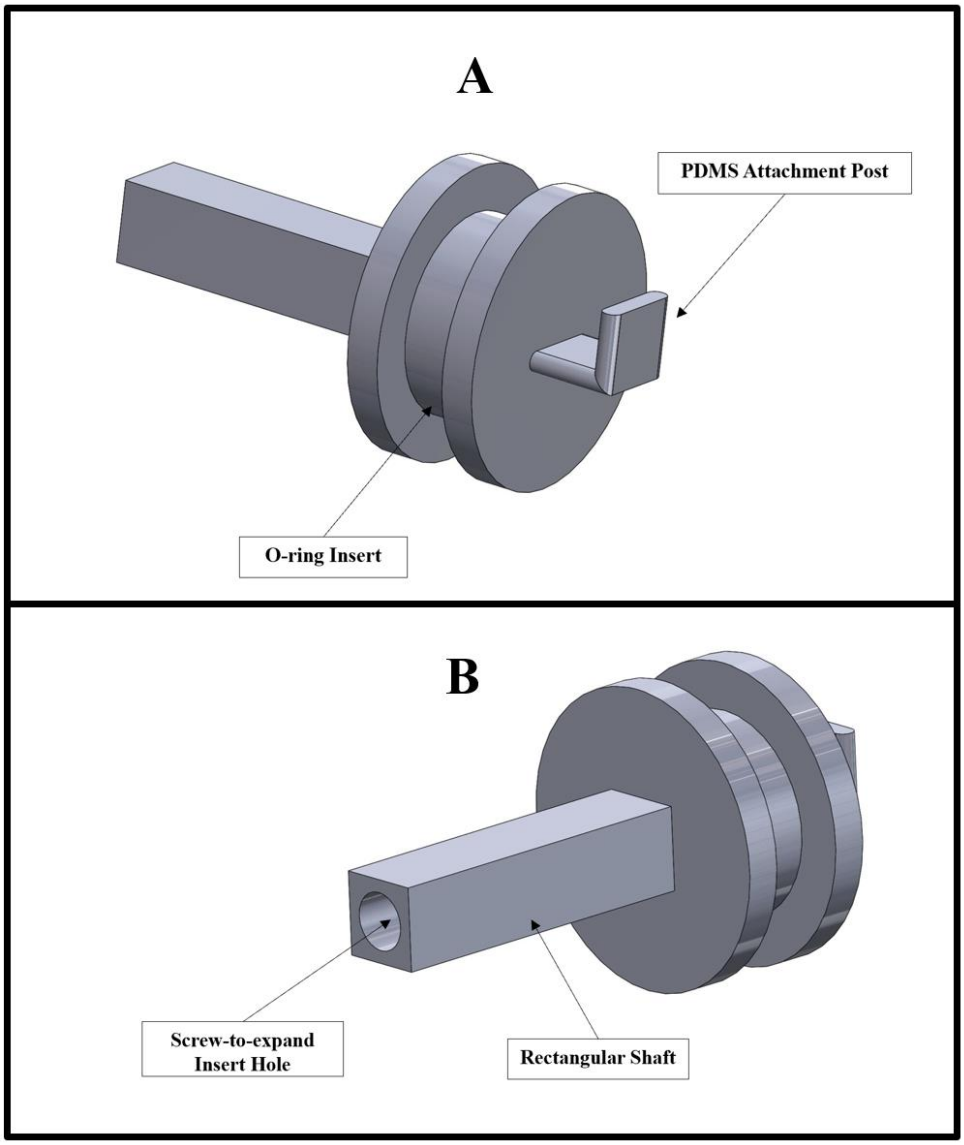

Figure 20. Motor Shaft Design with Key Features.

(A) Front-side view. (B) Rear view of shaft.

3.2.4. Housing Unit Design

In order for the system to be able to work under microgravity conditions, it must be attached to the stage of the RPM. To do this, the components needed to produce the stretching must be on an even surface, completely fixed, and must operate independently as a system (Figure 21). To accomplish this, a housing unit has been designed to act as a secure platform that can then be attached to the stage of the RPM (Figure 22).

The flask has been designed with bottom screw insert attachments, so the corresponding holes have been designed into the housing unit so that the culture flask can be screwed into the stage in a fixed position within the flask fixture. Similarly, the actuator has its own section to sit on at the opposite end of the stage in the actuator fixture. In this position, the actuator can be clamped down using a designed mounting bracket unit to fix the actuator from the top down to ensure it is completely flat against the stage. Another feature is the small hole in the center of the actuator fixture, and this is for the actuator cord to enter the bottom compartment and this will also prevent damage to the cord. The second component to the housing unit is a detachable bottom compartment which will contain the electrical components needed for the system. This also allows for protection of the electrical components from the humid environment of the incubator. The housing unit has been designed with several screw attachment holes that will allow the entire platform to seal tightly together and attach to the stage of the RPM using bolts.

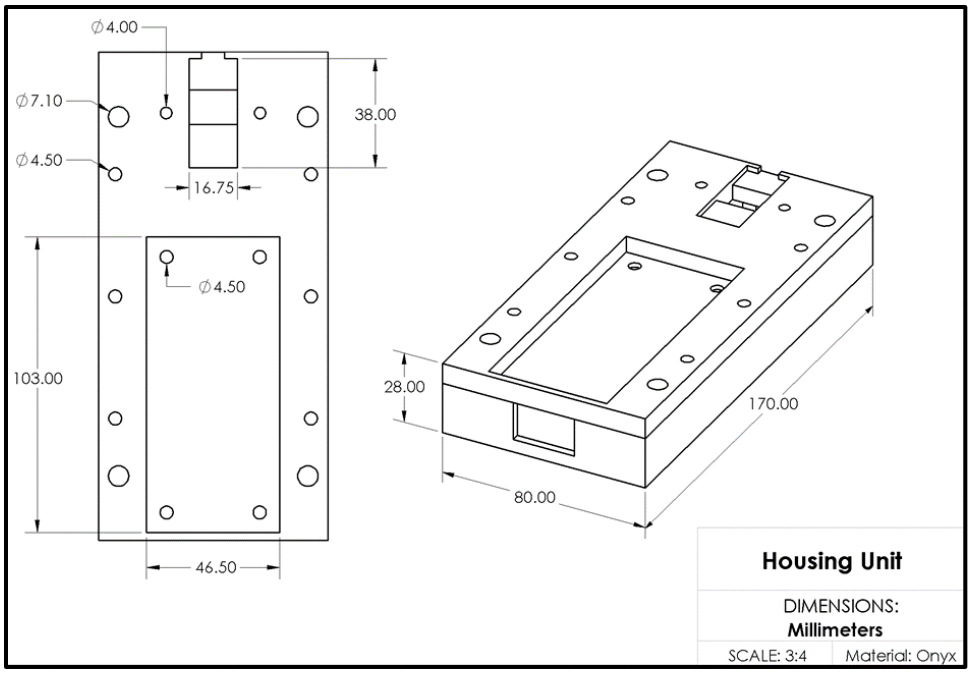

Figure 21. Housing Unit Drawing Specifications.

Schematic of the housing unit illustrates the design of the part.

The material selection for the construction of the housing unit consisted of choosing a 3D print filament that would be suitable under humid and dynamic environments. The complexity of the design also called for a printer that could accurately generate the part according to its specifications. For these reasons, the material chosen was Vero White printed using the Objet printer by Stratasys [35]. This material could easily be acessed for printing and it is able to be sterilized using an alcohol based spray which is important in preventing contamination.

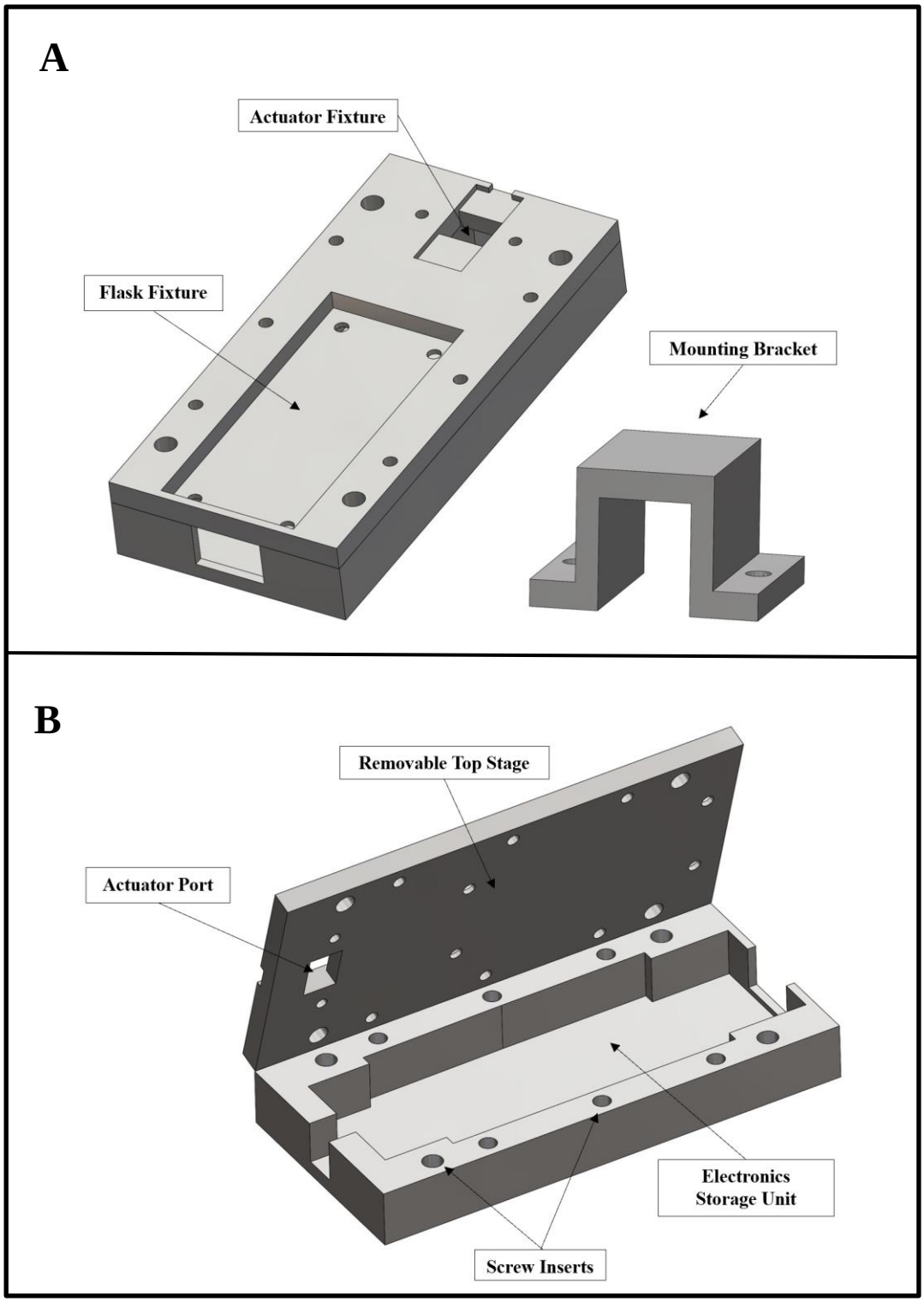

Figure 22. Housing Unit Key Features.

(A) Top stage of the housing unit. (B) Bottom compartment with key features.

3.2.5. System Assembly

The system assembly consists of all the components required for the bioreactor to function as a strain device (Figure 23). The actuator is clamped in two positions, one using the posterior attachment fixture, and the other through the use of the mounting unit directly on top of the motor.

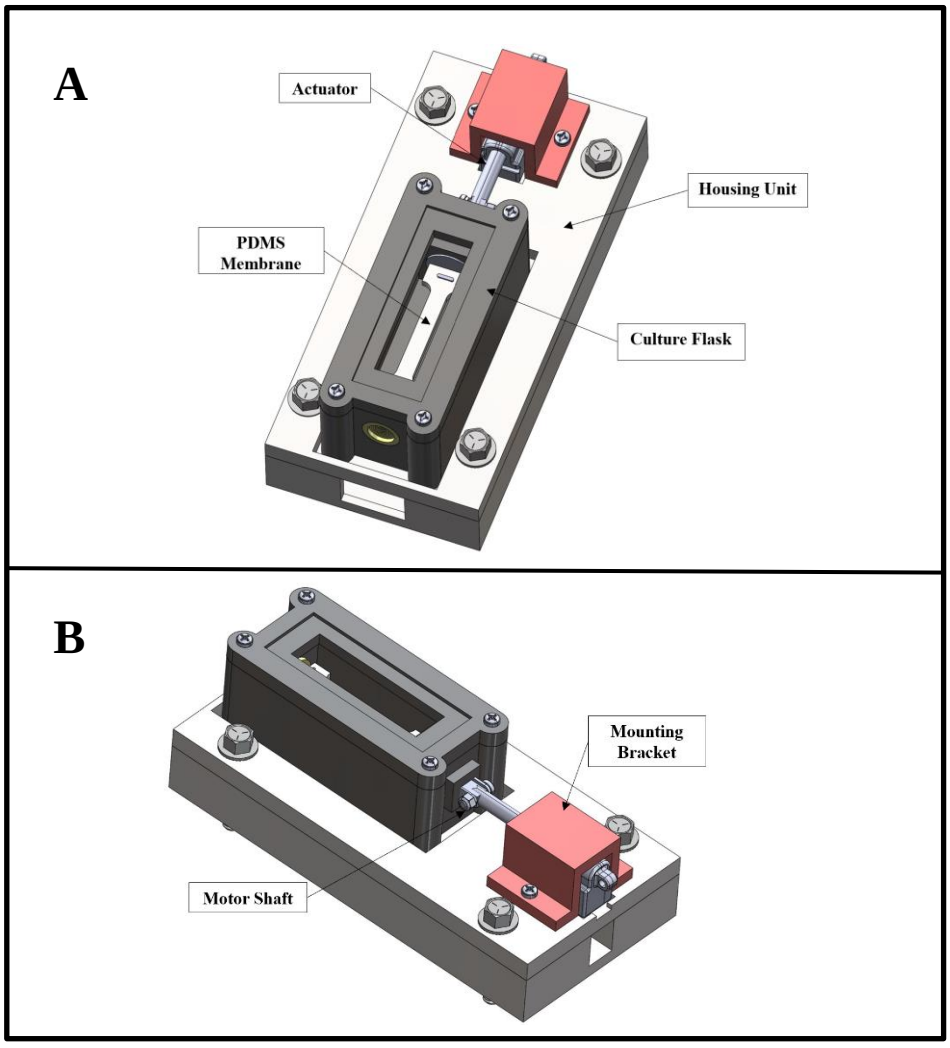

Figure 23. Bioreactor System Model Components.

Bioreactor completed CAD model viewpoints. (A) Top. (B) Isometric.

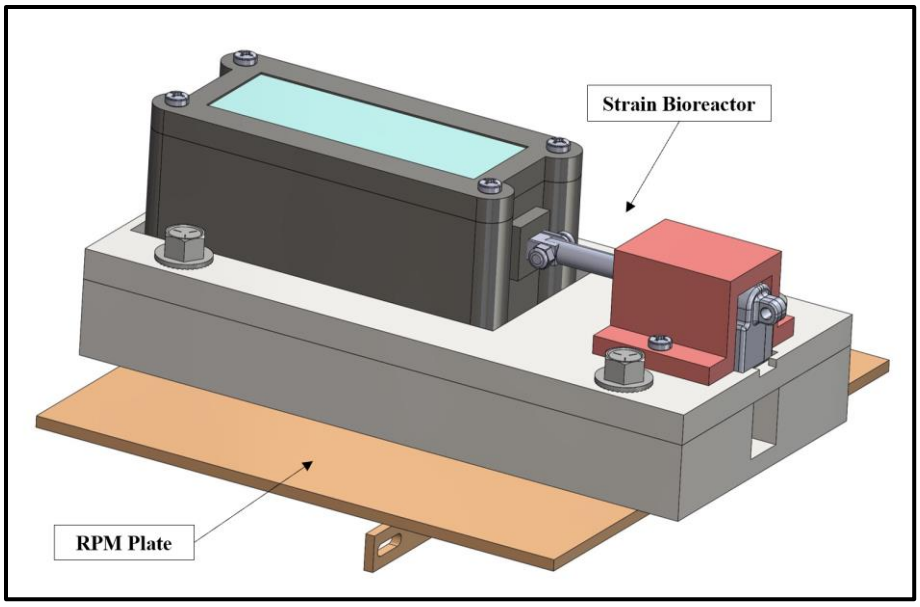

Figure 24. Final Bioreactor Device CAD Model.

Device shown as a CAD model and is attached to a custom RPM plate.

The actuator is connected to the motor shaft through screw insert within the rod of the shaft and a nut. The shaft goes through the entry site inside the flask and attaches to the dynamic side of the membrane, while the other is fixed on the PDMS post. The lid seals the culture flask from the top orientation and a viewing platform allows for real time showing of cyclic stretching. The addition of a custom-made plate used for the RPM was the final addition to the model design of the complete bioreactor (Figure 24). The use of this plate allows for a secure attachment of the strain device to the RPM and this system has been fitted with the exact specifications provided by Airbus. The bioreactor device could be put together as dictated by the previous system assembly model (Figure 25). The mechanical properties of the device proved to work well for this application since none of the high stress components, such as the PDMS post and shaft clamp, were damaged or deformed as a result of uniaxial cyclic stretching for long periods of time.

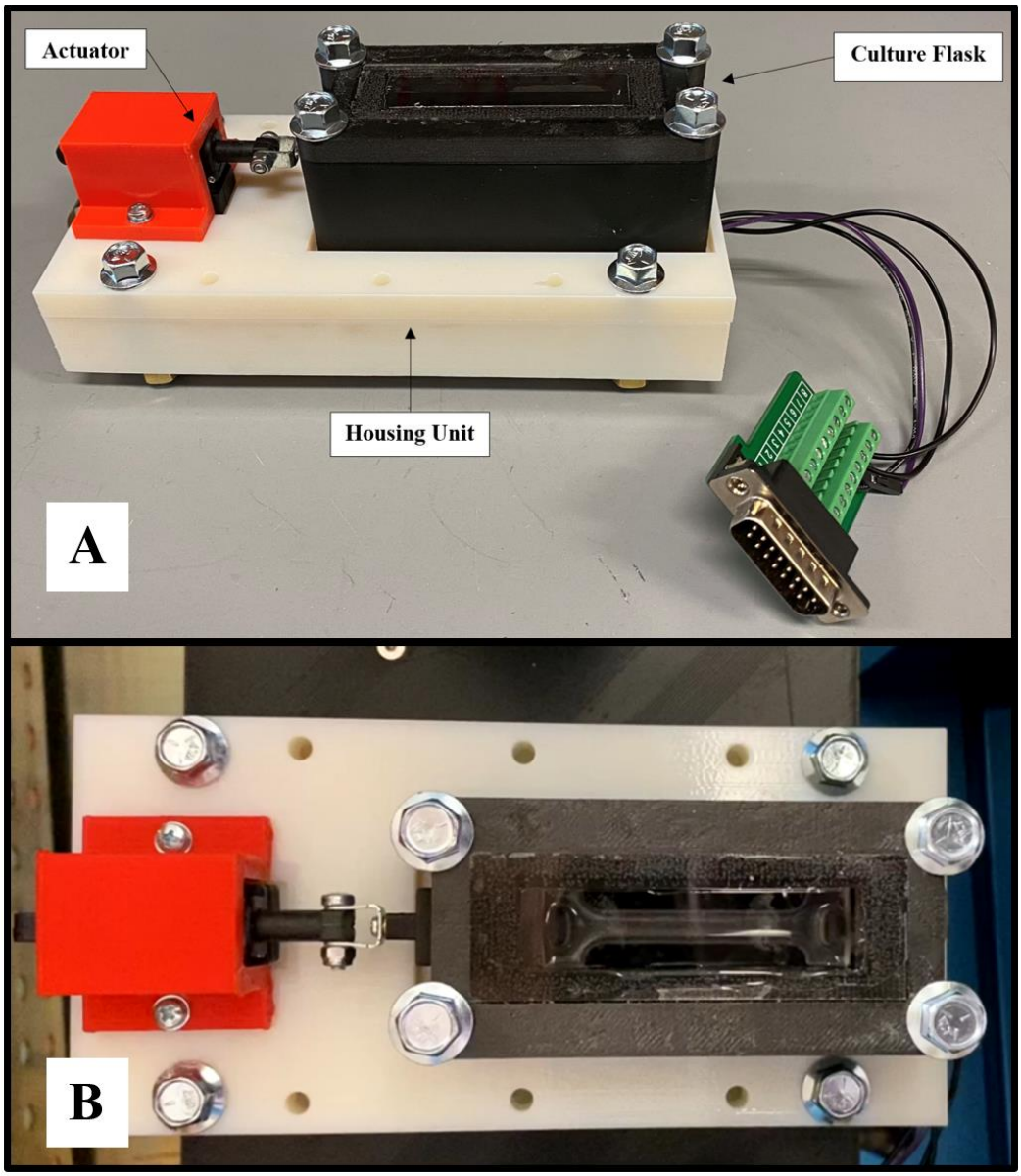

Figure 25. Constructed Bioreactor Final Device.

(A) Side view illustrating bioreactor main components. (B) Top view of system.

This system put together with all of its corresponding components was able to function consistently function as a strain device, and this was further validated with its attachment to the RPM (Figure 26). The device is able to securely attach to the Random Positioning Machine via the custom-made plate and this allowed for a secure base attachment which also limited vibration of the system while under experimentation.

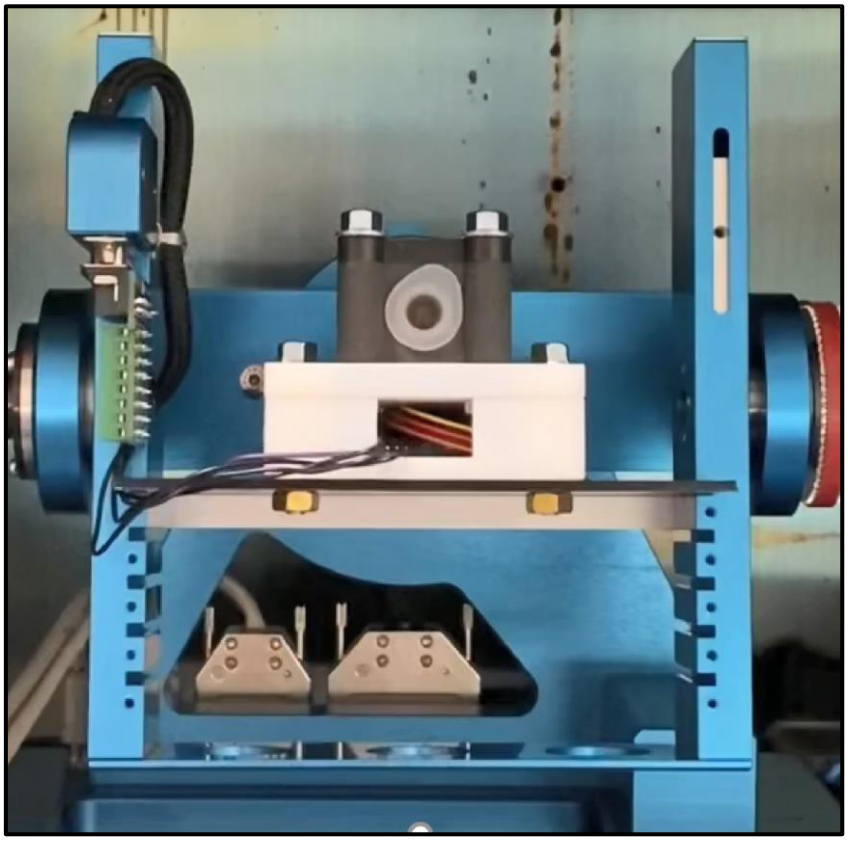

Figure 26. Final Bioreactor Device Attached to the RPM.

The device is fixed onto the plate using screws attachments while it is connected to the native DB15 port of the RPM.

3.2.6. Biocompatibility Testing

The materials used to construct the device were tested for biocompatibility since they are coming into direct contact with living cells. To accomplish this, a direct contact cytotoxicity testing protocol was used in order to determine cell viability and the proportion of healthy cells. Once formulating the final device and verifying that it is fully self-contained, the direct contact test was performed using cell culture medium solution. The cell culture flask containing all of the necessary interior components, including the motor shaft with its O-ring and PDMS membrane, were filled with cell MEM Alpha complete culture medium solution to its maximum volume and then sealed using the lid. The cell culture flask was then be placed inside an incubator under standard incubation conditions of 37 °C, 5 % carbon dioxide, and 100% relative humidity for 72 hours. Once the 72-hour incubation time has elapsed, the cell culture medium solution was extracted from the flask to be used for cell culturing and cytotoxicity testing. The cytotoxicity testing procedure used an alamarBlue™ Cell Viability Reagent Protocol. AlamarBlue™ is a resazurin-based solution that uses the reducing ability of living cells to quantitatively measure cell proliferation. In living cells, Resazurin is reduced to resorufin by accepting electrons from NADPH, FADH, FMNH, NADH and cytochromes, and as a result viable cells will turn red in [36].

The assay protocol consisted of culturing cells in a 96-well plate under several different controls versus the experimental (Figure 27). On the well plate, the columns characterized by B3-G3 and B4-G4 were filled with fresh cell culture media and alamarBlue™ reagent (only added immediately before measurement), and this will act as the untreated control group. The next two columns of B5-G5 and B6-G6 will consist of the first experimental group, which will consist of cells, 72 hour-soaked cell culture medium

in a T25 flask, and alamarBlue™ reagent. The next two columns of B7-G7 and B8-G8 contains the second experimental group consisting of cells, the 72-hour-soaked culture medium solution in the Onyx material flask, and alamarBlue™ Reagent. Lastly, B9-G9 and B10-G10 contains the final experimental group consisting of cells, the 72-hour-soaked culture medium solution in the Rigid Resin material flask, and alamarBlue™ Reagent [37]. The remaining wells around the samples will be filled with DI water to optimize the humidity.

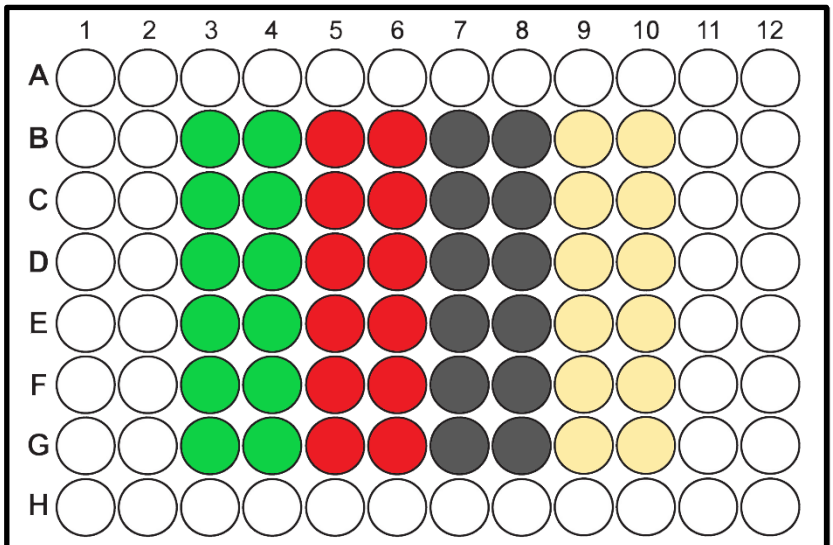

Control	T25 Soaked	Onyx Soaked	Rigid Resin Soaked
B3-G3 B4-G4	B5-G5 B6-G6	B7-G7 B8-G8	B9-G9 B10-G10

Figure 27. Biocompatibility Assay 96-well Plate Schematic.

The wells colored in green contained the control of fresh culture medium. The second control group consisted of the red wells, which was medium soaked in a T25 flask for 72 hours. The first experimental group is highlighted in gray and this was the Onyx culture flask soaked medium, while the yellow wells correspond to the Rigid Resin culture flask-soaked MEM alpha.

For this assay, cells were plated in cell culture medium in a two-fold dilution series into the 96-well plate seeded at 5,000 cells/well, containing 100 μL of cells and culture medium, and was incubated overnight under standard incubation conditions for 24 hours. After this time has passed, the cell plate was removed from incubation and 10 μL of media solution was removed from all the wells. Next, 10 μL of alamarBlue™ reagent was added to the appropriate wells, making the total volume 100 μL in each cell well. Once adding alamarBlue™, the 96-well plate was placed in the incubator for 2 hours. After this, fluorescence readings were taken at excitation/emission 560 nm/ 590 nm wavelength using a plate reader to determine cell viability. Data from the plate reader was extracted and used to show the relationship of cell viability of the experimental compared to the control group of untreated cells, which was performed by plotting the fluorescence versus the experimental condition of cell number [37].

3.2.7. Gas Permeability Assay

In order to ensure that the constructed bioreactor allowed for a suitable environment for cells to grow, a final bioreactor test needed to be conducted. This was a gas permeability assay, which was conducted to confirm that enough gas exchange occurring through the flask. To do this, a comparative study was performed between the constructed culture flask and a standard T25 flask.

For this experiment, MEM Alpha incomplete culture media was used as the solution and dissolved oxygen was the variable being measured. A stock solution of culture medium was taken directly from storage and warmed in the water bath at 37 °C for 30 minutes. The media was then removed and placed into an Erlenmeyer flask and the initial concentration of dissolved oxygen content was measured using a PinPoint II Dissolved Oxygen Monitor.

The initial dissolved oxygen in solution from freshly opened culture medium was found to be 3.4 ppm. After this, a rubber stop plug was used to seal the Erlenmeyer flask containing the medium; however, a modification was made to the stopper to allow for a Pasteur Pipette to come into contact with the medium solution and this enabled the use of nitrogen gas sparging of the culture medium solution. The solution was flushed with nitrogen mixed gas with 5% carbon dioxide and 1% oxygen for 10 minutes and this allowed the initial dissolved oxygen concentration of the solution to drop to 0.3 ppm (Figure 28).

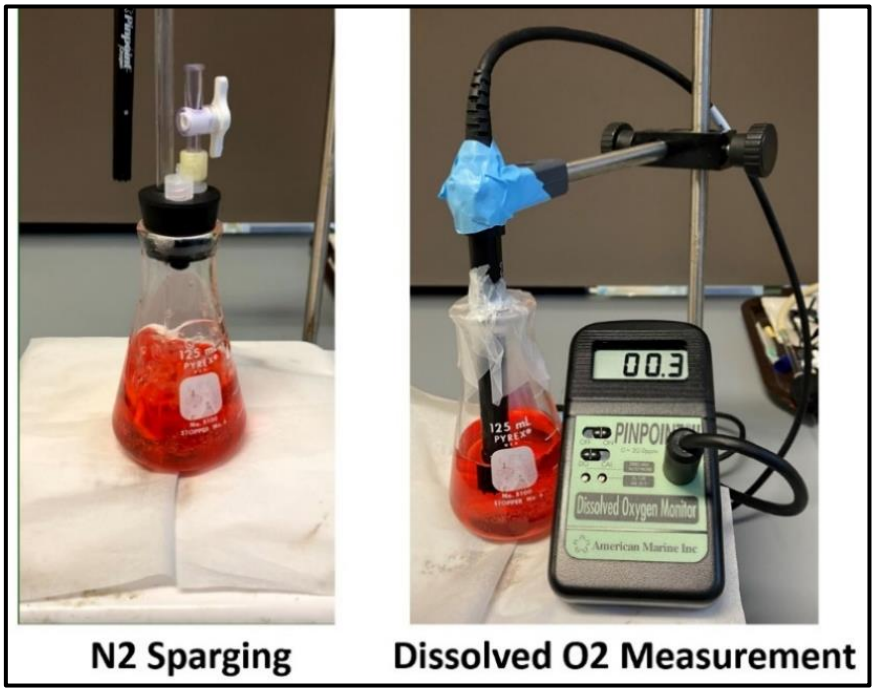

Figure 28. Gas Permeability Assay Set-up.

Nitrogen sparging of culture medium solution (left). Initial dissolved oxygen concentration of flushed medium taken with Pinpoint II Dissolved Oxygen Monitor (Right).

After this, 35 mL of the flushed culture medium was added to both a standard T25 flask and the custom-made bioreactor flask. The T25 flask was sealed with its standard aerated vent cap while the custom flask was sealed using a silicone vent cap and Tegaderm™ and then placed in the incubator to equilibrate (Figure 29).

The dissolved oxygen content in each of the flasks was recorded every 30 minutes using the monitor and the experiment was completed once the initial dissolved oxygen content was retained. This experiment was performed in total three times and the dissolved oxygen values were recorded and averaged graphically.

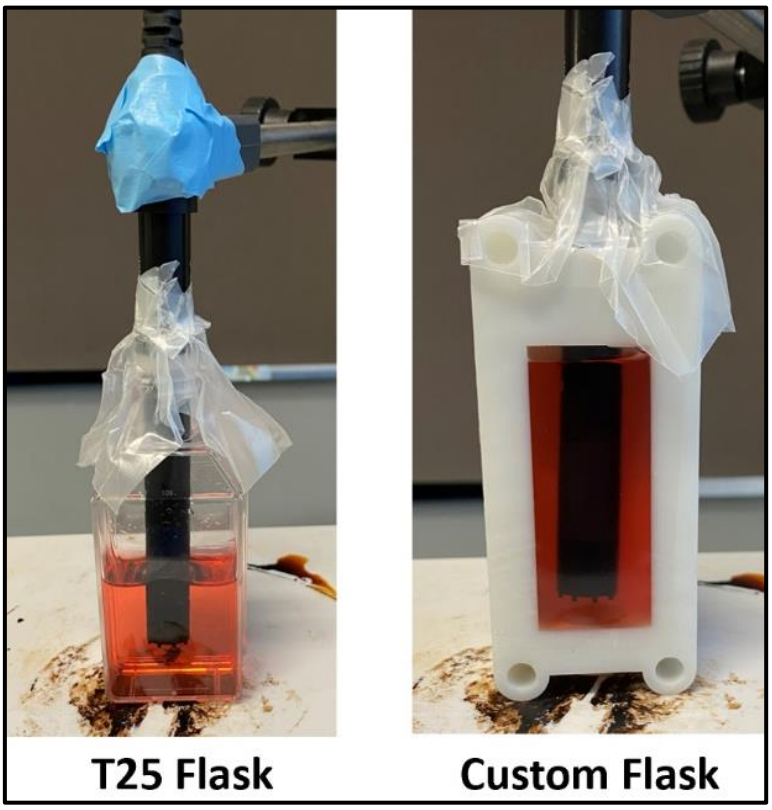

Figure 29. Dissolved Oxygen Measurement Set-up.

T25 Flask (Left) and Custom Flask (Right) were measured for dissolved oxygen concentrations every 30 minutes.

3.2.8. Actuation System

The electrical control system has undergone several iterations throughout the course of the project. The overall goal of the electrical control system was to be able to control the motion of the actuator remotely from outside the RPM, in addition to minimizing the total number of components inside the RPM. Reducing the number of components within the RPM allows for saving space and mitigating the risk of excess heat transfer to the ambient surroundings of the RPM. Since the RPM is within the incubator, the temperature and humidity must be precisely controlled. Excess heat transfer to the inner contents of the RPM could result in a temperature increase, such a temperature increase could be detrimental to the growth of the cells. The actuator selection was guided using the previous assumptions. The PQ12 Linear Servo was available in eighteen different configurations (R, S, or P), (30:1,63:1,100:1), and (6V or 12V). The configurations described correspond to the control type, gear ratio, and actuator voltage, respectively. The P actuators were selected as they possess a potentiometer feedback for position, speed, sensitivity, and end limits [38].

The P actuators need a servo control board in order to customize the response of the servo to a control signal. Due to this requirement, it was decided to use the LAC control board from Actuonix. The LAC control board is a stand-alone closed loop 10-bit PD controller specifically designed for Actuonix actuators. The LAC board responds to a specified control signal and uses an algorithm related to the PD controls to instruct the motion of the servo [39]. Although this closed loop system can be controlled on its own using an external potentiometer and a power source, the control board is compatible with 5 different control signal types (Figure 30). The control signals can be additionally broken into two separate categories digital, and analog control signals. The three available digital

control signal types are 1Khz PWM (Pulse Width Modulation), standard RC, and USB control using LabVIEW. The two available analog control are 4–20 mA, and 0–3.3V [39].

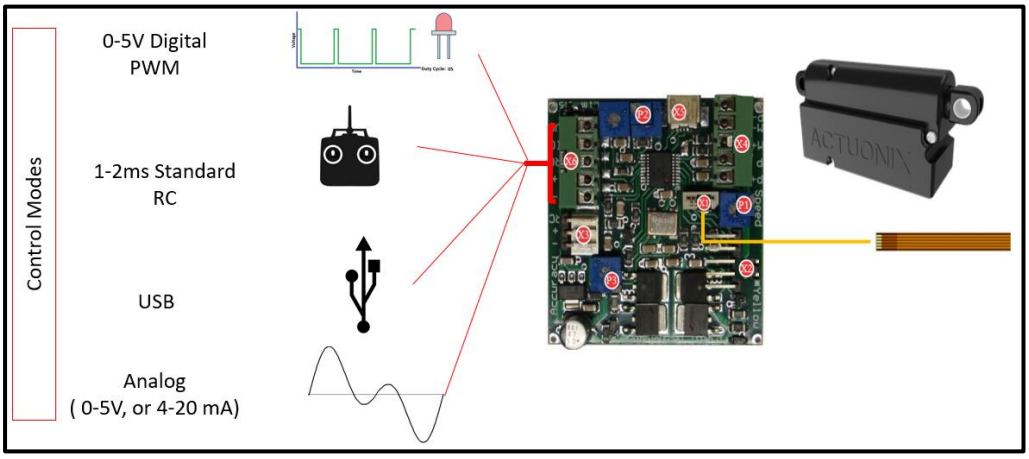

Figure 30. LAC Control Modes.

Various control types suitable for the Actuator controlled by the LAC board. [39]

The diversity of the control signal types provides the user with flexibility when designing the electrical system. The initial decision to use the PQ12 (P) type actuator, with the LAC Control Board already provided the ability to control position, and speed; thus, any additional components added to the electrical will be aimed at triggering the servo response at precise intervals to coordinate loading for sustained amounts of time. Keeping this assumption in mind it was determined that a standard microcontroller, and or microcomputer could be readily programmed, and prototyped to fit the demands of the system.

Originally, it was decided to use a standard Arduino Uno as the coupled microcontroller in the system. The Arduino Uno is widely used and comes at a great price point. Due to widespread use of the microcontroller, it is compatible with many electronics and provides easily accessible ways to add functionality to the microcontroller with extra

peripherals. Additionally, Actuonix provides a setup guide to introduce using an Arduino Uno coupled to the LAC Control Board to control any of their linear Actuators. The Arduino Uno can provide the LAC Board with a PWM control signal at the specified frequency [39], [40]. Although the microcontroller has a built-in analog to digital converter the decision to use PWM over an analog control signal was made based on the principle that PWM uses dramatically less power in comparison to a continuous waveform. Servos draw a great deal of current regardless of the control signal, however using a continuous waveform would mean that the servo is always on, while PWM quickly flips between on and off at different rates to simulate the same effect as an analog signal. Thus, using a continuous waveform where the servo is always on could lead to additional heat generation due to the increased power demands. The Arduino Uno uses 0-5V logic level voltage, therefore the PWM Signal will have the same 5V amplitude [40]. The LAC board states on its datasheet that the inputs are 5V tolerant however the percentage duty cycle may vary, thus it was advantageous to switch to a 3.3V logic level [39].

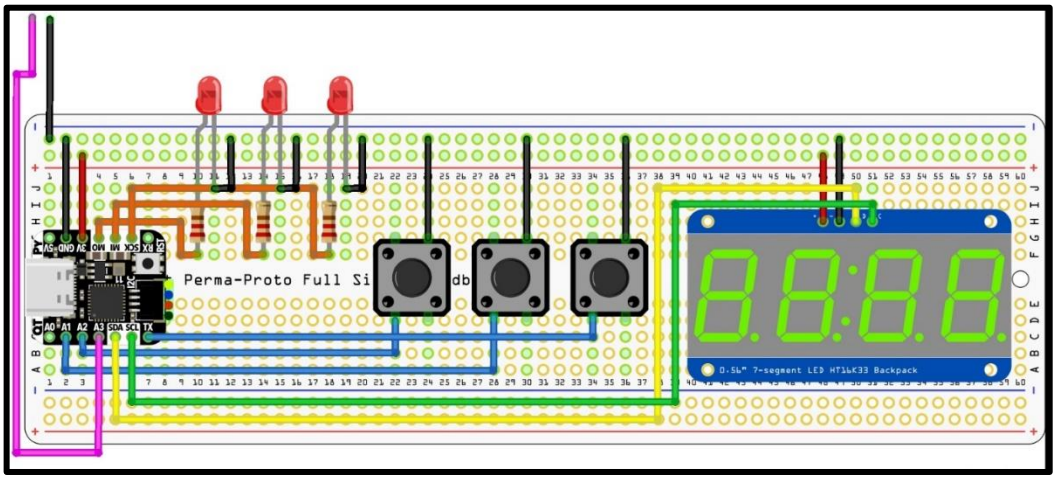

Figure 31. Initial Circuit Schematic Diagram.

The electrical control system breadboard includes the Adafruit QT Py microcontroller, control input buttons, and an LED display.

A final approach has been implicated for the electrical system, and a series of changes have been made to improve upon the previous system (Figure 31). The largest change is the microcontroller being used to control the system, shown on the far left of the circuit diagram. This new microcontroller is the Adafruit QT Py which uses the SAMD21E18 chip replacing the Arduino Uno which uses the ATmega328P chip [41]. A comparison of the two microcontrollers and their key metrics (Table 2).

Microcontroller	**Adafruit QT Py**	**Arduino Uno R3**
Logic Level Voltage (V)	3.3V	5V
Clock Speed (MHz) / Bits	48 MHz / 32-bit Processor	16 MHz / 8-bit Processor
RAM (KB)	32 KB	2 KB
Flash Memory (KB)	256 KB	32 KB
Dimensions (length / width)	(0.81 in / 0.70 in)	(4.00 in / 2.00 in)
Price ($)	$6.00	$23.00

Table 2. Comparison of Microcontrollers.

The Adafruit QT Py and Arduino Uno R3 were compared to one another to distinguish the most suitable option for the electrical system.

As shown in the table, the Adafruit QT Py outperforms the Arduino Uno in terms of speed, memory, form factor, power consumption, and price. Reducing the form factor can allows the entire control system onto one PCB or Breadboard. The system works by pressing one of the tactile push buttons shown to tell the servo to perform a preprogrammed continuous cyclic strain of (10%, 5% and 1%) from left to right respectively [41]. Once the button is pressed the corresponding LED will illuminate to indicate the system is in action

and the strain rate being applied is displayed on the seven-segment display shown on the far right of the board. The display uses the I2C protocol to communicate with the microcontroller while the buttons and LED are all digital inputs and outputs, respectively. The pink and black wires that are not routed to any part of the board are connected to the Actuonix LAC Board where the black wire is the common ground, and the pink wire is for 0-3.3V 1KHz pulse width modulation. This part of the system is to remain outside of the incubator with an additional 12V 2A power supply for the servo driver. The four connections being made to the LAC board will be connected intermediately serially using a set of two DB15 breakout boards and a VGA cable [39], [41]. The RPM has two native DB15 serial ports which is why this approach is employed (Figure 32).

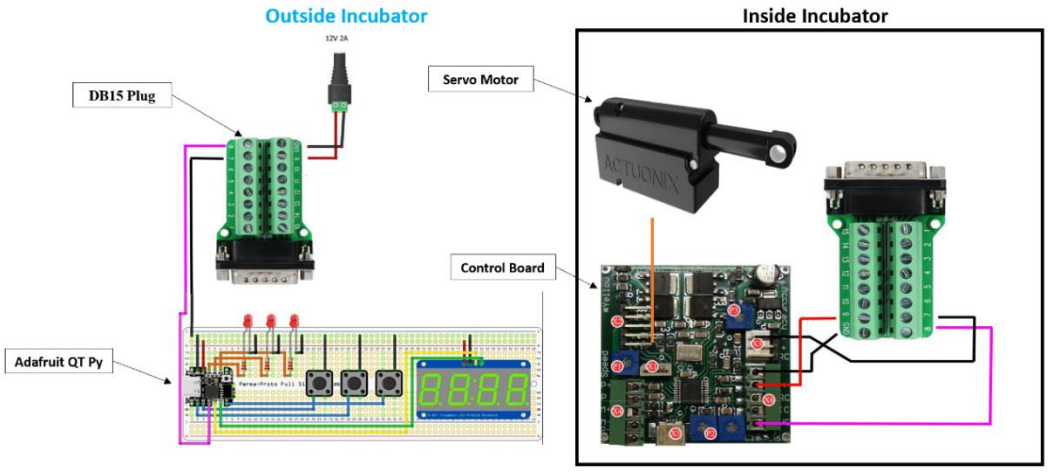

Figure 32. Circuit Schematic Diagram for Electrical System.

This system allows for the main circuit board to function outside of the incubator while only the actuator and control board are required to be inside.

To test actuator performance, the microcontroller coupled with the LAC control board, and servo was probed with an oscilloscope between the LAC boards input and microcontroller output to ensure that the voltage of the control signal matches the expected

behavior of the servo. The circuitry components were tested using Arduino programming and the mathematical calculations used to write the code were formulated.

3.3. Aim 3

The goal of this specific aim was to use the constructed device to conduct cell stretching experiments both under normal and reduced gravity conditions in order to verify that this bioreactor functions as it was designed. The device was able to operate effectively as a strain device while attached to the RPM and it can be utilized as a viable research tool. This aim illustrated the evaluation and analysis of the effect of strain under reduced gravity in regard to cell morphology.

3.3.1. Cell Culture

There have been numerous studies performed using bioreactor devices to apply mechanical strain on cells, yet this has not been performed while under microgravity conditions. The type of cell that has been decided to evaluate mechanical loading effects on bone under reduced gravity are osteoblasts. This cell type was selected since there have been many studies conducted using osteoblasts for cell stretching experiments due to their cytoskeletal properties and phenotype expressions once being subjected to strain [42]. Additionally, osteoblasts were chosen since they are able to directly assess how a lack of gravity affects cellular development for bone growth [43]. The selected cell line for experimentation was the MC3T3-EI (mouse) cell line. This cell line is a spontaneously immortalized cell line that has acted as the standard model for normal osteoblast differentiation [44].

Murine pre-osteoblasts from the cell line MC3T3-E1, subclone 4 were the cells used for all experimentation. The cell line was cultured in Gibco brand MEM alpha

supplemented with 10% fetal bovine serum, and 1% penicillin/streptomycin at 37 °C in 5 % carbon dioxide, and 100% relative humidity [45]. During experimentation, cells were passaged every 4 days, refreshed with new cell culture medium at day 2, and were split at a ratio of 1:6. Health of the cells was regularly monitored via phase contrast microscopy (Figure 33).

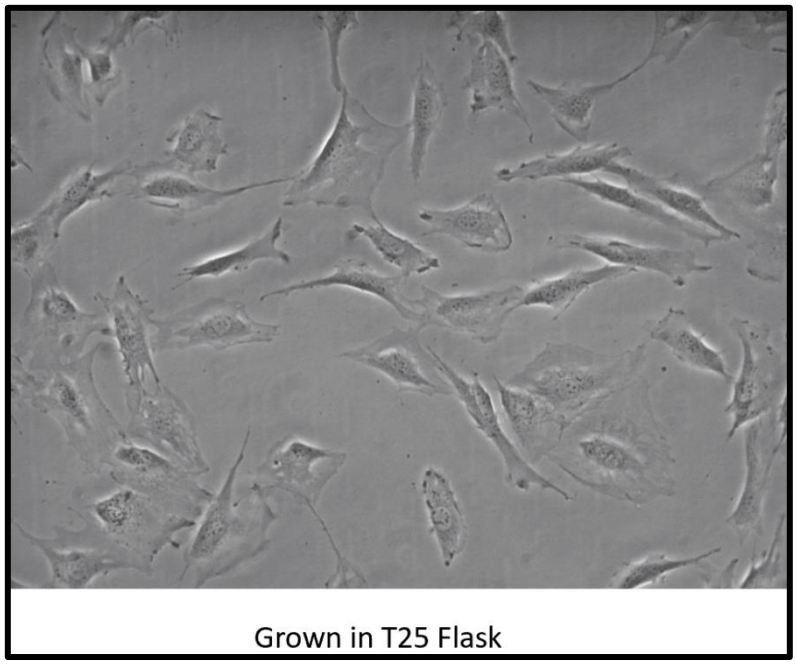

Figure 33. MC3T3-E1 Cell Culture.

Cells were cultured in a T25 Flask and seeded at 400,000 cells/mL. Image was taken 24 hours after splitting.

3.3.2. Cell Adhesion

Cellular adhesion assays using the grown cell line consisted of utilizing a cellular adhesion protein to attach cells to the PDMS membranes used for cell stretching experiments. The process first began with the formulation of PDMS membranes, as previously described. The formulated membranes were then soaked in 70% isopropyl alcohol for 1 hour to allow for swelling and the elimination of debris. Following this, the

membranes were dried and then soaked with DI water for 24 hours, and then washed three times with DI water. Once the PDMS membranes were cleaned from debris, they were sanitized via autoclave sterilization using a Getinge Autoclave on the pipette tips setting. Once sterilized, PDMS membranes were oxygen plasma treated using a Plasma Etch device for 2 minutes (power of 75 W). This was performed to increase the number of hydroxyl groups on the outer surface of the PDMS membranes to allow for enhanced protein attachment [46]. After this, the membranes were put into the biosafety cabinet and treated with UV light for 30 minutes for sterilization. The plasma activated and sterilized PDMS membranes were then treated with 100 μL of sterile 0.1% gelatin in water solution to the gauge area [47]. The membranes were then placed into the incubator for 24 hours to allow the gelatin solution to dry and attach to the surface of the membranes.

Once the gelatin solutions had properly adhered to the PDMS membranes, cells could be added to the surface [48]. Cells were grown to confluency and split using 0.25% trypsin solution. Cells were counted using a hemocytometer and the number of cells per mL was calculated. A volume of 500 μL of the cell solution was added to the surface of each PDMS membrane by drops and 230,000 cells were added to the gauge area [49]. The cell solution was left on the PDMS membranes for 30 minutes to allow the cells to adhere. After this, the remaining volume of the petri dish was filled with fresh culture medium [47]. Cells were grown for 24 hours to allow attachment and spreading and imaged using phase contrast microscopy (Figure 34).

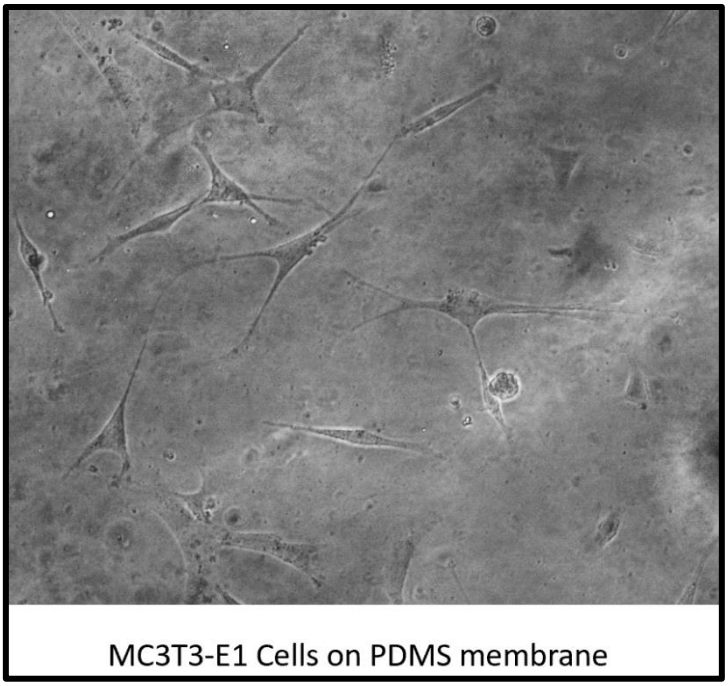

Figure 34. MC3T3-E1 Cellular Adhesion to PDMS.

Cells were seeded to gelatin coated PDMS at 230,000 cells and imaged after 24 hours.

3.3.3. Cell Morphology

Morphological testing on cells was conducted to determine how strain under different conditions affects cellular growth and development. Cells were cultured under several testing conditions for 48 hours (Table 3). The control group was to culture cells under standard normal gravity conditions. This will consist of utilizing a modified culture flask design that is fully enclosed since there will be no stretch occurring (Figure 35). The first experimental group cultured the cells solely under microgravity conditions, and this group also made use of the same modified flask. Using these additional flasks enabled the user to run more tests at once, which will ultimately save time for the completion of the project. The second experimental group consisted of culturing cells while subjecting them to uniaxial cyclic strain using the bioreactor at 5%.

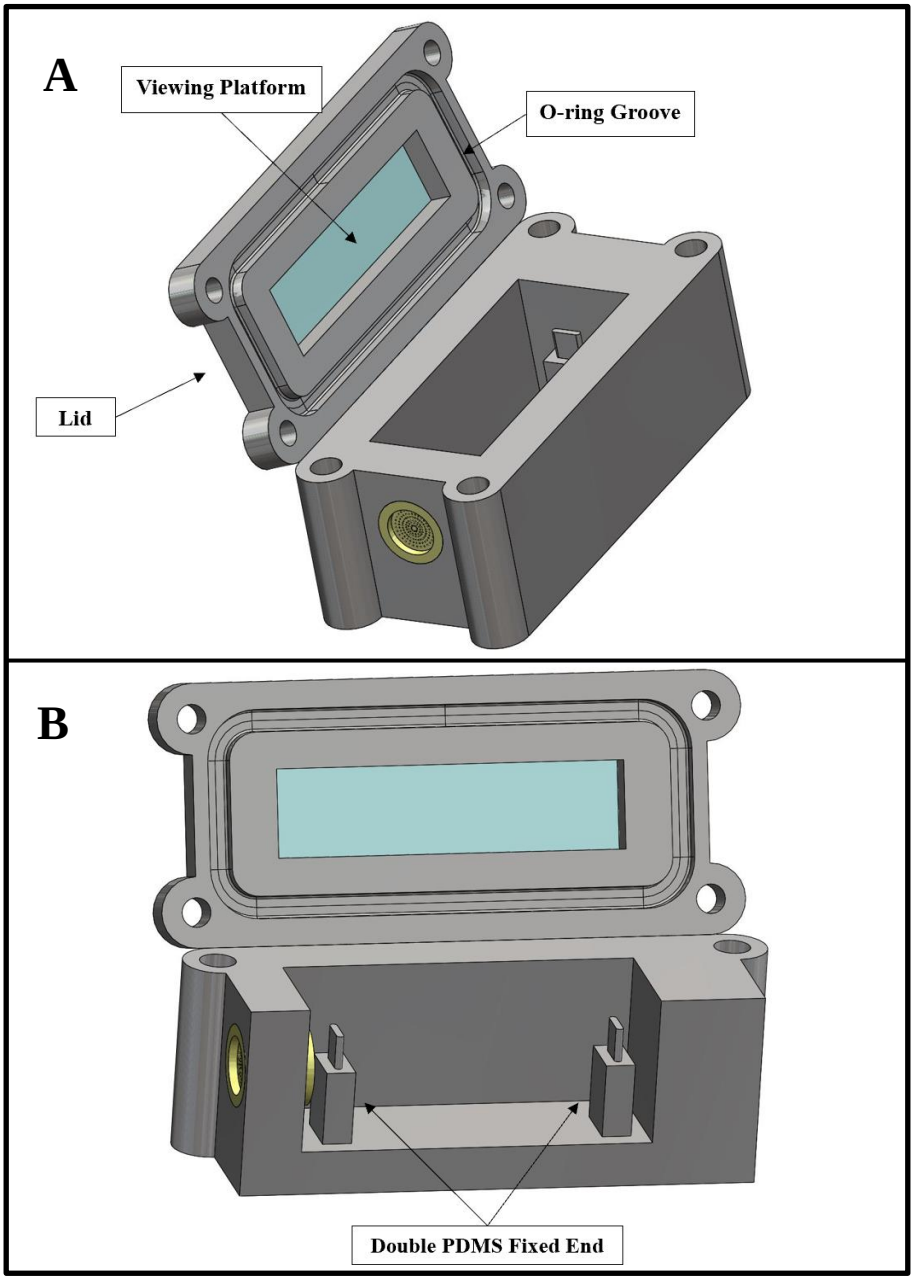

Figure 35. Static Culture Flask Design.

(A) Exterior features include the gas exchange port and sealing lid. (B) Interior components, illustrate the double PDMS attachment sites.

This value was chosen since previous studies have used a range of 0.25%-12% using this particular cell line. The final experimental group provided the information proposed by the hypothesis and will evaluate the cell culture of osteoblasts under both microgravity and uniaxial strain at the same corresponding values. Each of the testing conditions were completed in triplicate (passages 19-21) in order to obtain statistically relevant data.

	Testing Conditions	**Condition Duration**	**Flask Type**
Control	Standard Gravity	48 hr Static	Static
Experimental 1	Microgravity	24 hr Static, 24 hr RPM	Static
Experimental 2	Uniaxial Strain – 5%	24 hr Static, 24 hr Strain	Stretch
Experimental 3	Microgravity & Uniaxial Strain – 5%	24 hr Static, 24 hr RPM + Strain	Stretch

Table 3. Testing Conditions for Cellular Experimentation.

Cells were subjected to a control group of standard gravity and the experimental groups of microgravity, uniaxial 5% strain, and microgravity coupled with 5% uniaxial strain.

In order to conduct the experiments in both an efficient manner, while also utilizing the same passage of cells for each experiment, a modification was made to the device application with the Random Positioning Machine. The design of a new RPM plate allowed for the microgravity and the microgravity strain groups to be run on the device during the same time (Figure 36). The weight addition of the extra culture flask did not affect the weight distribution across the plate since the bottom was securely bolted using screws and locknuts (Figure 37).

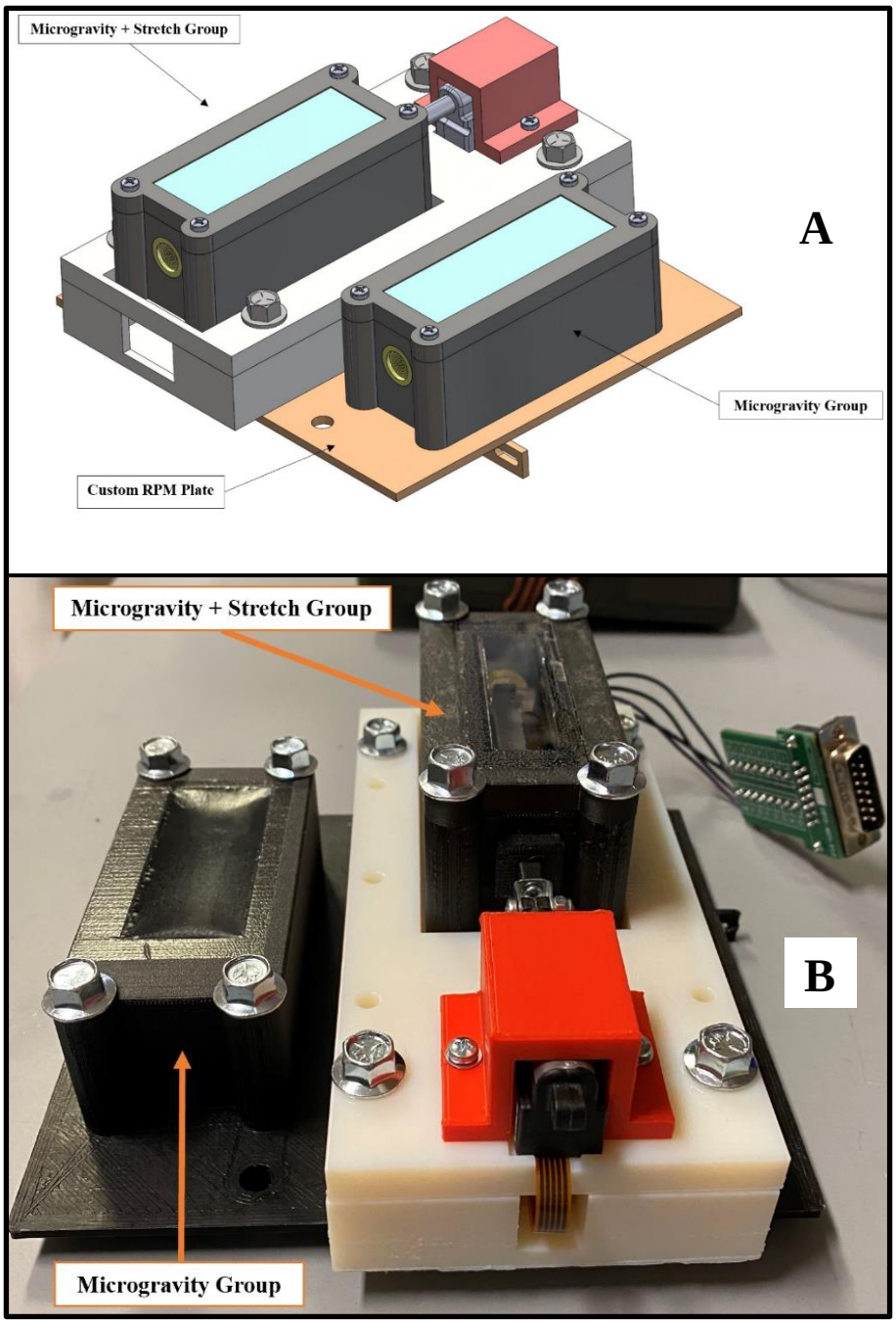

Figure 36. Dual Condition Bioreactor Set-up.

Fully functional bioreactor used to test microgravity and stretch microgravity groups. (A) Model design of system. (B) Constructed system.

The protocol for each of the groups consisted of seeding cells onto the PDMS membranes. Once adhered, the attached cells on the PDMS membranes were placed into the incubator for 24 hours to allow them to properly adhere to the membrane and acclimate to this new environment. The control group was incubated for an additional 24 hours and imaged. The first experimental group was subjected to microgravity conditions for 24 hours, and after this, images were taken of the gauge area. The second experimental group was stretched at 5% strain for 24 hours prior to taken images. Lastly, the final experimental group was subjected to stretching in microgravity and then images were taken under the microscope. The use of the 24-hour time period is to prevent the cells from becoming too confluent.

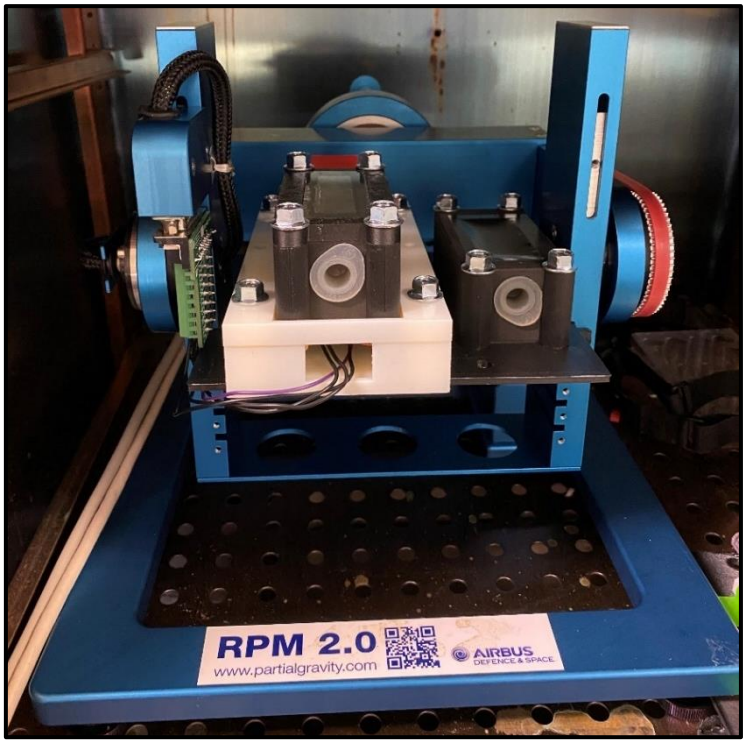

Figure 37. Dual Condition Bioreactor on RPM.

The final bioreactor device is attached to the RPM plate. Both the stretch device and microgravity group can be ran simultaneously.

Once the set-up was defined and the devices were prepared and sterilized, the experiments were conducted. After experimentation, to better visualize the cells, staining methods were employed. The PDMS membranes containing the treated cells were washed with 1X PBS three times and aspirated carefully. Next, a solution of 4% paraformaldehyde was prepared and the samples were submerged and washed for 1 hour to fix the cells. Following this, the paraformaldehyde solution was aspirated and disposed of and the samples were washed with 1X PBS three times. Samples were then stained using Hoechst 33342 1mg/mL stock solution (Thermo Scientific) with a working concentration of 1:1000 dilution and Alexa Fluor™ 647 Phalloidin stock solution of 200U/mL and a working solution of 1:200 dilution. Samples were soaked in this a mixed solution of the stains for 1 hour. After this, the samples were removed from the stain and washed with 1X PBS three times to wash away the stain. Imaging of the cells was conducted using confocal microscopy. The cells were imaged for each of the experimental groups and images were taken at a magnification of 10X with a 2X digital zoom.

CHAPTER 4

4. RESULTS

4.1. Aim 1

This aim illustrates the results for the design and formulation of an elastic membrane material that can be suitable for cyclic uniaxial stretching of cells.

4.1.1. Modelling Software Analysis Results

In order for the computational software to calculate the desired mechanical properties, the solver utilized 13 steps to allow the solution to converge. During each of these steps, the values of stress, strain, and the displacement can be shown on the membrane to indicate how the properties changed as a result of increased displacement. The value of displacement was selected to be 2.5 mm as an estimate to calculate the mechanical properties of the membrane if it were subjected to between 1-10% strain. This range of strain was examined since previous studies have utilized it to examine the effect of mechanical loading on bone cell development, and it is within the relevant biological limit [13], [50]. The result of the study indicated that this model using 2.5 mm displacement of this specific membrane allowed for uniformity in regard to stress, strain, and displacement while this was also shown during the progression of the displacement forces (Figure 38). The first outcome generated illustrated the stress in the form of von Mises stress. This form of stress corresponds to a single value that is able to incorporate multiple stress orientations according to the mesh parameters to yield a single value that can be compared to a tensile test data value of tensile stress.

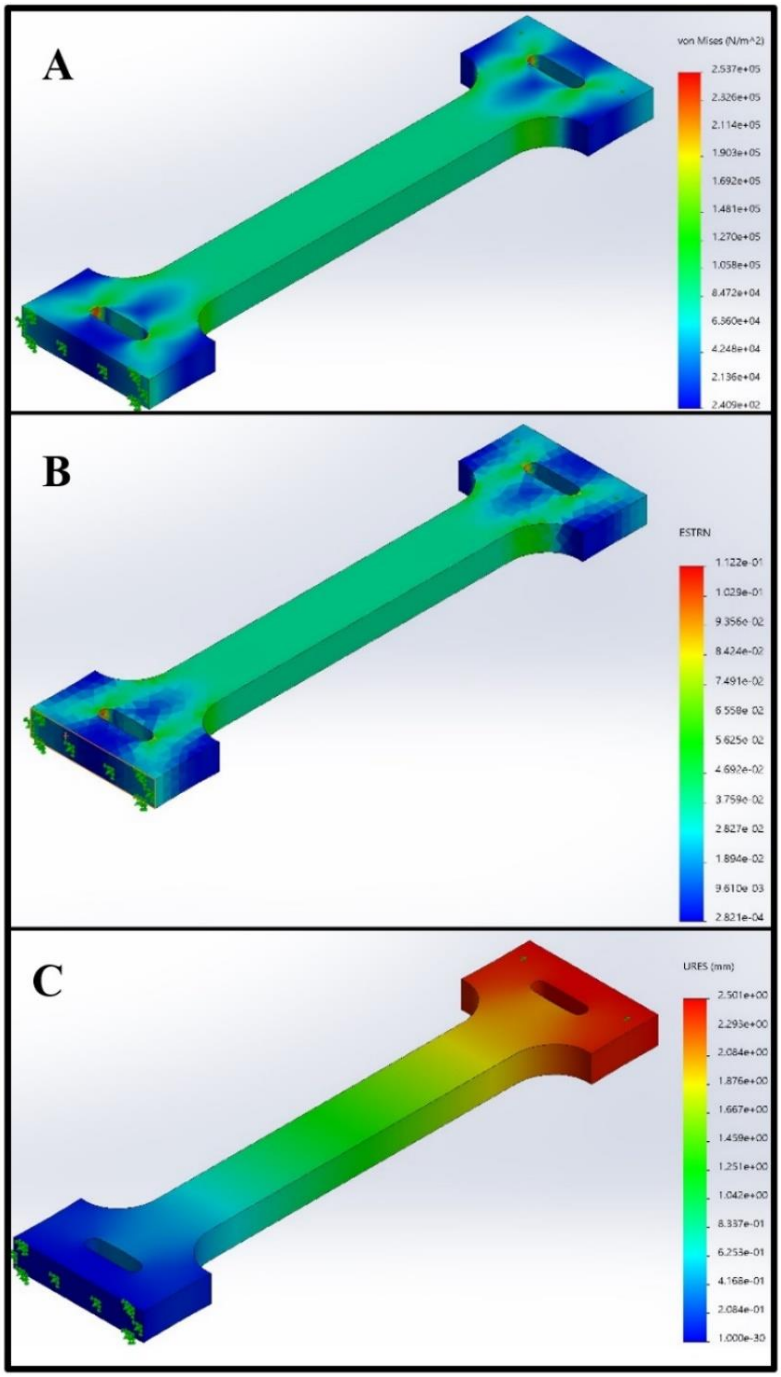

Figure 38. PDMS Modeling Software Analysis

This analysis consisted of inducing a 2.5 mm displacement to the dynamic end of the PDS membrane in SolidWorks. (A) Maximum stress. (B) Maximum strain. (C) Maximum displacement.

At maximum displacement, the von Mises stress showed to be uniform across the gauge length at an approximate value of 1.058e+05 Pa (Figure 38A). The solver also illustrated the engineering strain present on the membrane to be uniform across the gauge length at a value of 4.69% (Figure 38B). This value is within the required range of 1-10% strain which indicates that this design is suitable for uniaxial stretching. The plot illustrating the displacement also indicated that there is indeed uniformity in the central region of the membrane which further validates the use of this design as a substrate (Figure 38C). From these findings, the PDMS membrane was verified as a suitable model for testing.

4.1.2. PDMS Tensile Test Results

From the data obtained, the stress-strain diagrams were made to illustrate the mechanical properties of PDMS. The samples were plotted on the same plot (Figure 39) and then the mean was taken of their corresponding results to plot the average result (Figure 40). For the purposes of this project, the only area of interest lies in the linear elastic region of the plot where Hooke's Law can be applied to calculate the modulus of elasticity [51]. The PDMS samples showed linear behavior up to 30% strain and the elastic region was plotted and averaged for analysis.

The results indicated great consistency among the test samples, especially in comparison of the linear elastic region where the R^2 value of the average stress-strain plot was 0.999 to indicate that this was indeed a linear fit. To better understand how well the data fits the mechanical model, the tensile stress and strain can be compared to the von Mises stress obtained from the simulation [52].

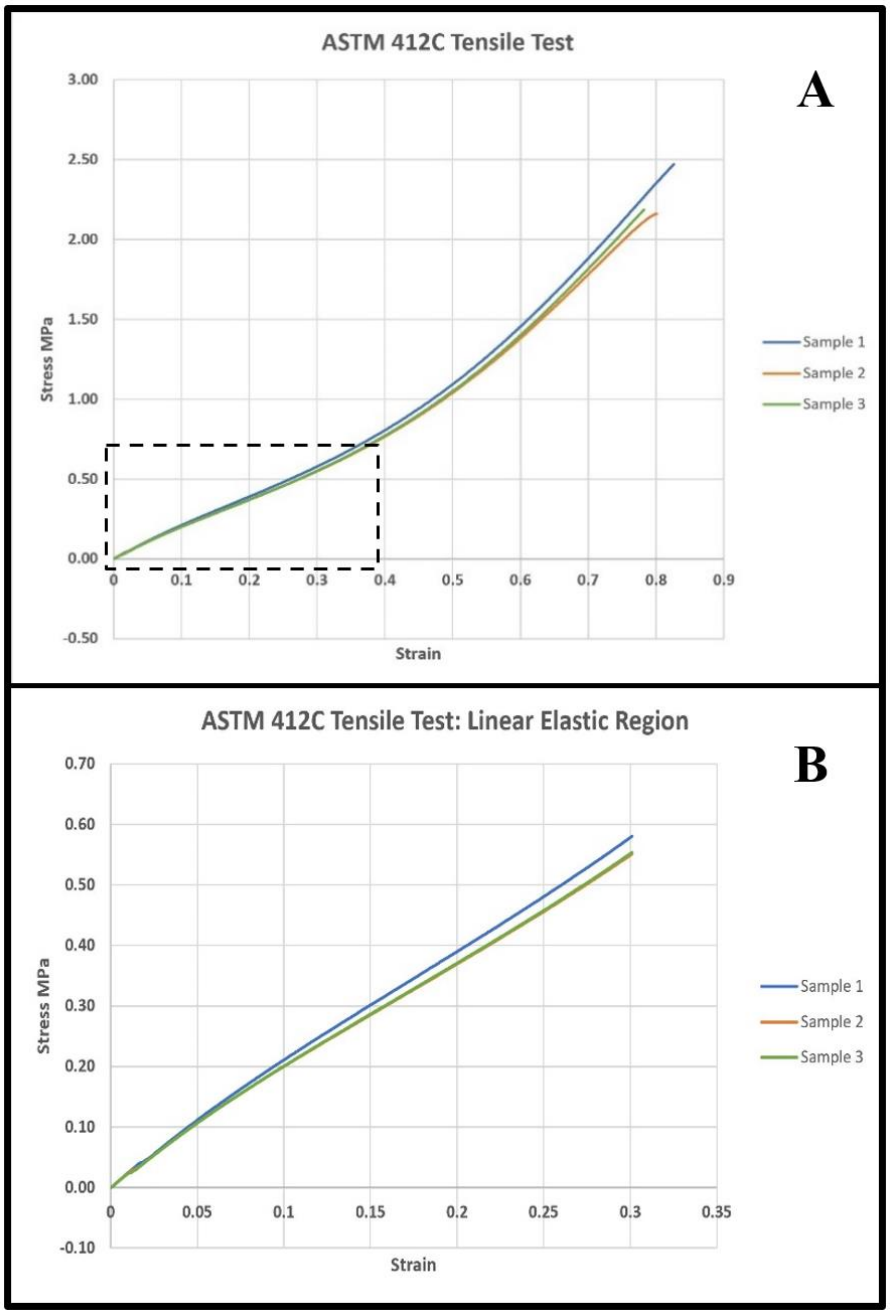

Figure 39. ASTM 412C Standard Tensile Test Results.

(A) Full stress-strain curve of the tensile test for all samples. The dashed box illustrates the linear elastic region of interest. (B) Stress-strain curve of linear elastic region.

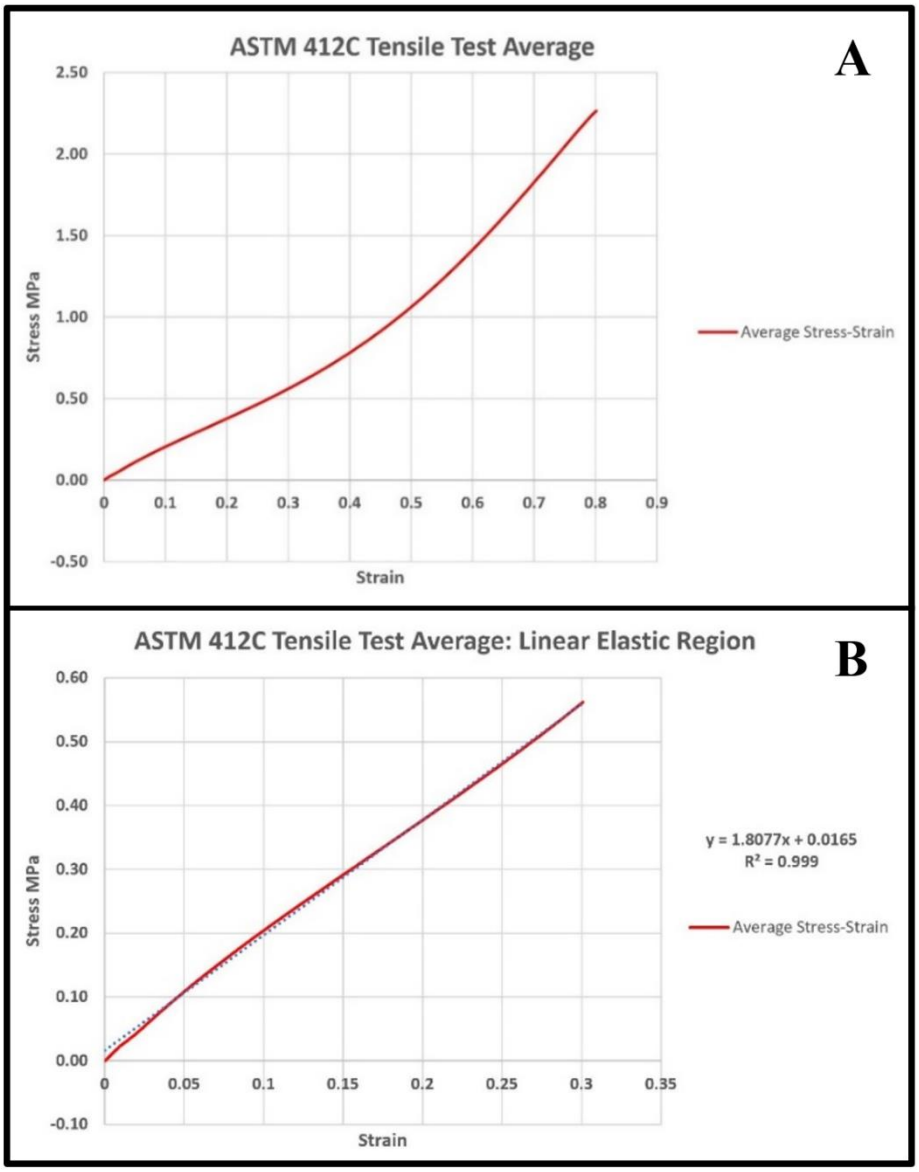

Figure 40. Averaged ASTM Tensile Test Results.

(A) Average stress-strain curve. (B) Average stress-strain curve from the linear elastic region. This curve was fit to a linear fit and the R^2 value was found to be 0.999 which indicated that the mechanical properties of PDMS are linearly elastic within this region.

From the simulation, the maximum strain value applied onto the membrane was approximately 5.5% with a corresponding von Mises stress of 0.1058 MPa. This information can be compared directly to the observed tensile data at approximately 5.5% strain which is found to be 0.1095 MPa. This similar result indicates that the model predictor for the custom-made membrane accurately depicted the actual mechanical properties of PDMS.

	Approx. Strain %	**Stress (MPa)**
Model	5.50%	0.1058
Tensile Result	5.50%	0.1095

Table 4: PDMS Tensile Results Comparison.

The model versus the experimental tensile test result illustrated that the model prediction compared similarly to the results obtained by the tensile testing of the PDMS membranes.

The purpose of performing a tensile test is to ensure that the mechanical properties are what is expected compared to the literature. According to the research in the literature conducted on PDMS, it has shown to cure differently depending on the substrate and curing temperature conditions [26]. The mold used for these experiments has not been used in previous studies, therefore there is a need to ensure that the mechanical properties of the formulated membranes through a tensile evaluation. To further validate the data, it was compared to a well-known PDMS study that utilized similar protocols and curing conditions (Figure 41) [29].

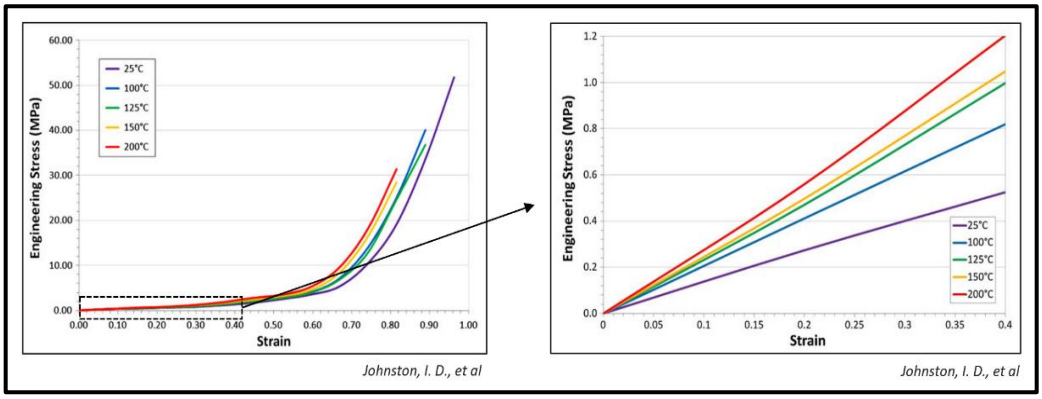

Figure 41. Tensile Test Results from Johnson, I.D.,et al.

Data from these results were taken in order to compare against the experimental data obtained. [29]

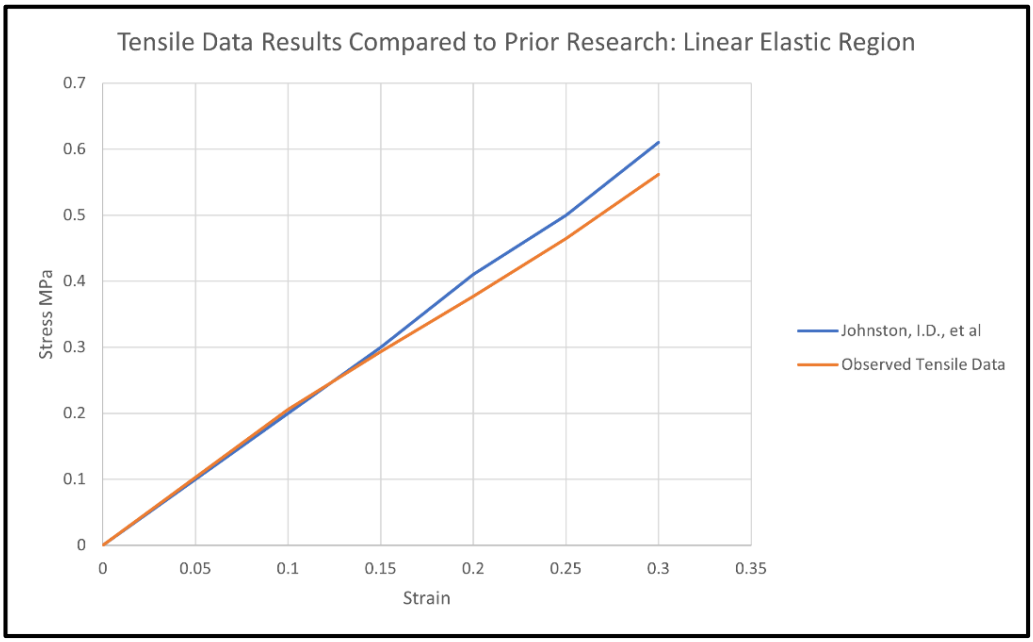

Figure 42. Observed Tensile Data Compared to Literature.

Comparison of the linear elastic region of the observed data versus the data obtained from Johnston, I.D.,et al. This illustrated that the formulated PDMS membranes behaved similarly compared to a well-known study. [29]

The linear elastic regions were plotted against one another and it was shown that linear fit was quite similar to the experimental data (Figure 42). This information indicates that the mechanical properties of the formulated PDMS are justified, which will allow for precise control of adjusting strain parameters on the membrane. Overall, the resulting data from specific aim 1 was able to indicate that the mechanical properties of the PDMS were suitable compared to both the mathematical model and the work from others in the field.

4.1.3. PDMS Strain Characterization Results

In order to analyze the consistency of the cyclic stretching, each of the samples were analyzed during 5 separate elongation and retraction cycles, then averaged to obtain the value of strain during the cycle. Once obtaining the data for each of the samples, the samples were analyzed through the use of a one-way ANOVA analysis in order to determine if there was a difference between the different PDMS samples according to their elongation and retraction cycles (Figure 43). The analysis indicated promising results, in that when comparing the different specimens using an alpha of 0.05 using a 95% confidence level that the p-value was found to be 0.7977, which indicates that there is no statistical difference between the strain values. This information is able to show that the mechanical properties of the PDMS membranes are suitable for the application of cyclic stretching, while achieving the desired amount of predicted strain using this substrate stretching system.

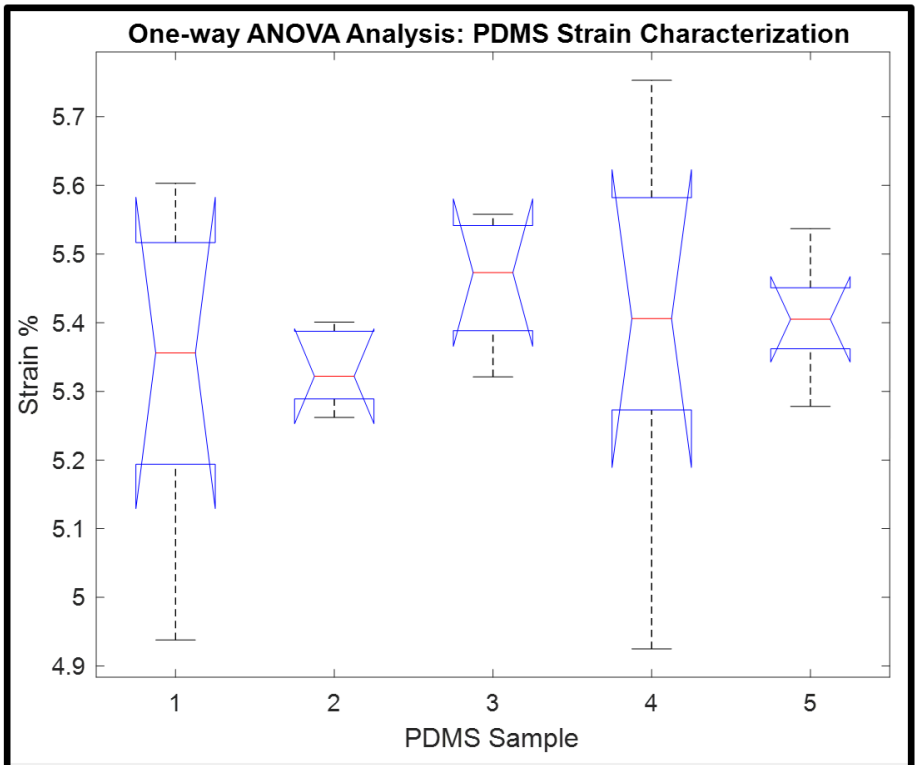

ANOVA Table

Source	SS	df	MS	F	Prob>F
Columns	0.05832	4	0.01458	0.41	0.7977
Error	0.70725	20	0.03536		
Total	0.76557	24			

Figure 43. ANOVA One-way Analysis of PDMS Strain Characterization.

Results indicated no statistical differences between the samples, indicating consistent cyclic strain. Error bars represent the range and interquartile range.

4.1.4. Fatigue Testing Results

The results indicated that this desired amount of strain did not appear to yield any permanent deformations on the PDMS membranes after 72 hours of constant cyclic stretching (Figure 44). This shows that the properties of the membranes within this linear elastic region allow for the mechanical loading and relaxation without altering the geometry of the specimens. This is important since cells growing on this membrane will need to be cultured for periods of days and the ability to apply constant and uniform cyclic stretch is crucial.

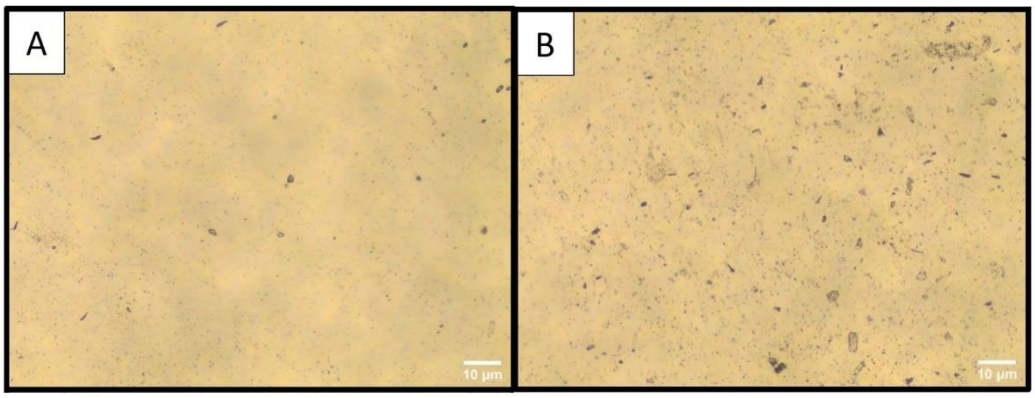

Figure 44. Fatigue Testing Results.

PDMS membrane samples were cyclically stretched for 72 hours at 5% strain. (A) Illustrates the surface of PDMS membrane before testing. (B) After fatigue testing no structural damage was found in the samples. Black specs are micro bubbles and were found to be <10um which is not significant in size to cause for damage while stretching. Images taken using Olympus CKX53 on 10X magnification.

4.2. Aim 2

This aim illustrates the results pertaining to the development of a novel bioreactor capable of applying uniaxial strain on cells while subjected to micro/partial gravity conditions governed by a Random Positioning Machine.

4.2.1. Biocompatibility Testing Results

This experiment was performed in total of three times. The data was extracted and evaluated using an ANOVA one-way analysis of variance to determine if there were biocompatibility differences comparing the groups (Figure 45). The statistical analysis was conducted using an alpha of 0.05 under a 95% confidence level. The results were plotted using a boxplot and the statistical analysis yielded a p-value of 0.1014. This information indicates that there are no statistical differences between the groups in regard to the fluorescence measurements at 590 nm. This result indicates that the cell viability amongst the groups is comparable and that there appears to be no cytotoxic effects from the components used to construct the custom-made bioreactors. The bioreactor components coming into contact with cells proved to be biocompatible under these condiotions, which indicated that this system and the materials used are suitable for cell culture.

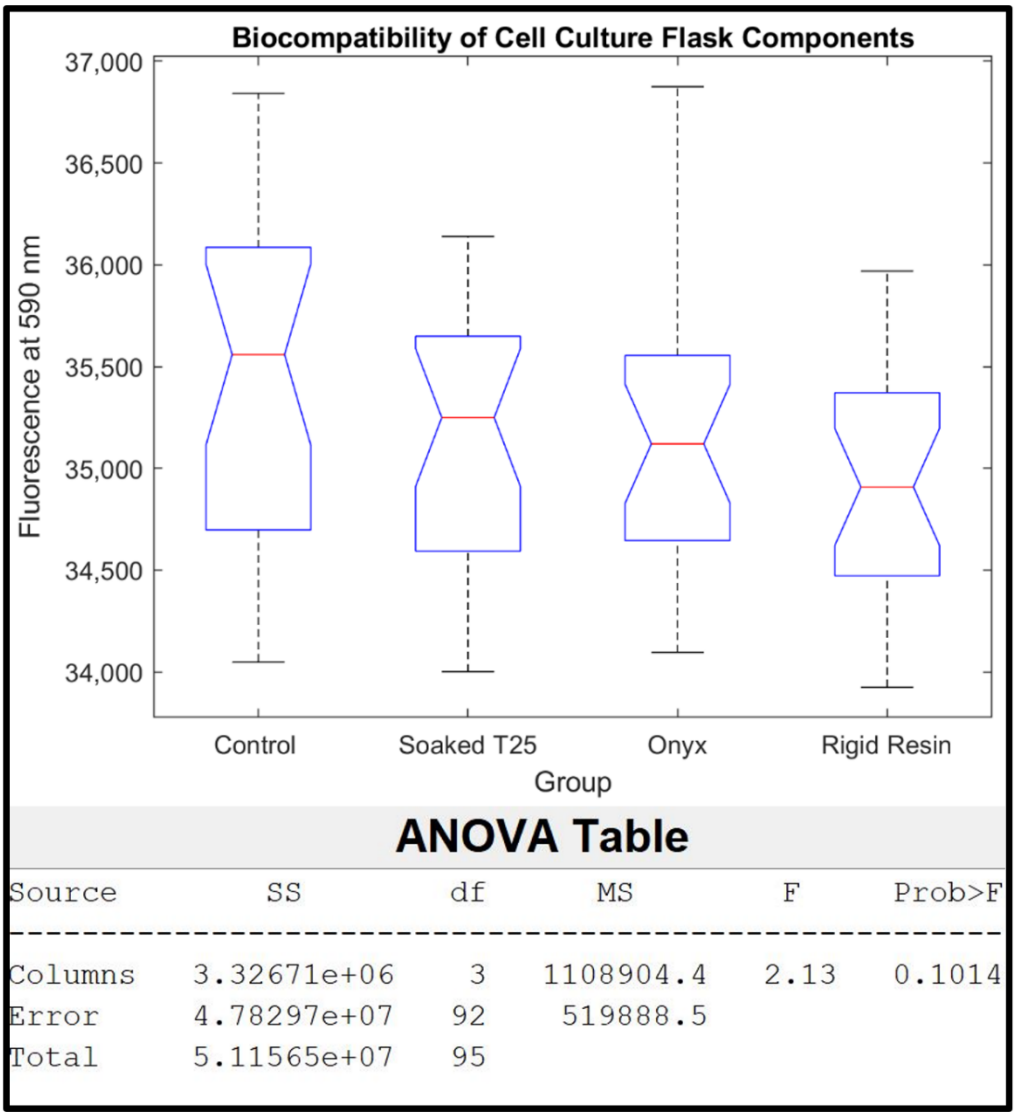

ANOVA Table

Source	SS	df	MS	F	Prob>F
Columns	3.32671e+06	3	1108904.4	2.13	0.1014
Error	4.78297e+07	92	519888.5		
Total	5.11565e+07	95			

Figure 45. ANOVA One-way Analysis of Flask Biocompatibility.

The results indicated a p-value of 0.1014 which corresponds to there being no statistical differences between the groups. This finding illustrates that all the interior bioreactor components are biocompatible.

4.2.2. Gas Permeability Assay Results

The averaged plots from the three trials of experimentation were graphed to illustrate the dissolved oxygen equilibration of the culture flasks and were plotted indicating the oxygen (ppm) over time (Figure 46). The results showed that both the T25 culture flask and the custom-made flask were able to reach the initial dissolved oxygen concentration at 180 minutes and were 3.5 and 3.4 respectively at this time point on average. After this point, both of the dissolved oxygen levels plateau over time and there is no change in concentration. These results indicate that the custom-made culture flask is allowing sufficient gas exchange compared to a standard T25 culture flask.

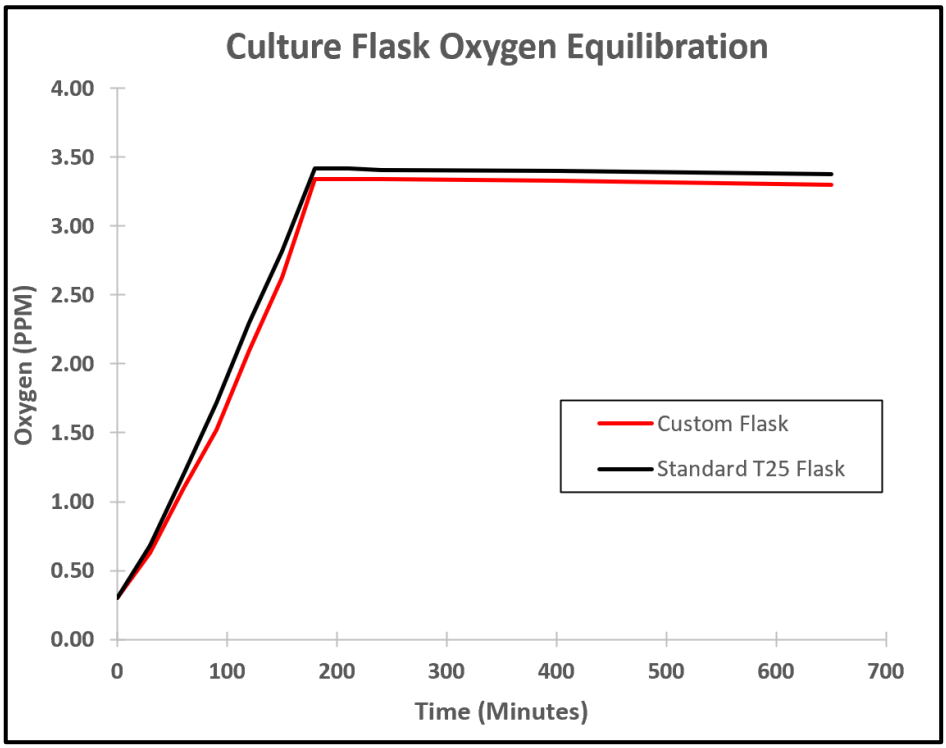

Figure 46. Average Dissolved Oxygen Concentration Over Time.

This was a comparative study to determine the average dissolved oxygen concentration equilibration in culture medium over time for a Standard T25 and the Custom Flask. Average dissolved oxygen concentration of the flasks compared similarly with one another at 180 minutes.

4.2.3. Actuation System Results

The actuator performance was examined by coupling the microcontroller with the LAC control board. The actuator was probed with an oscilloscope between the LAC board input and the microcontroller output. This was done to confirm that the voltage of the control signal matches the expected behavior of the servo (Figure 47).

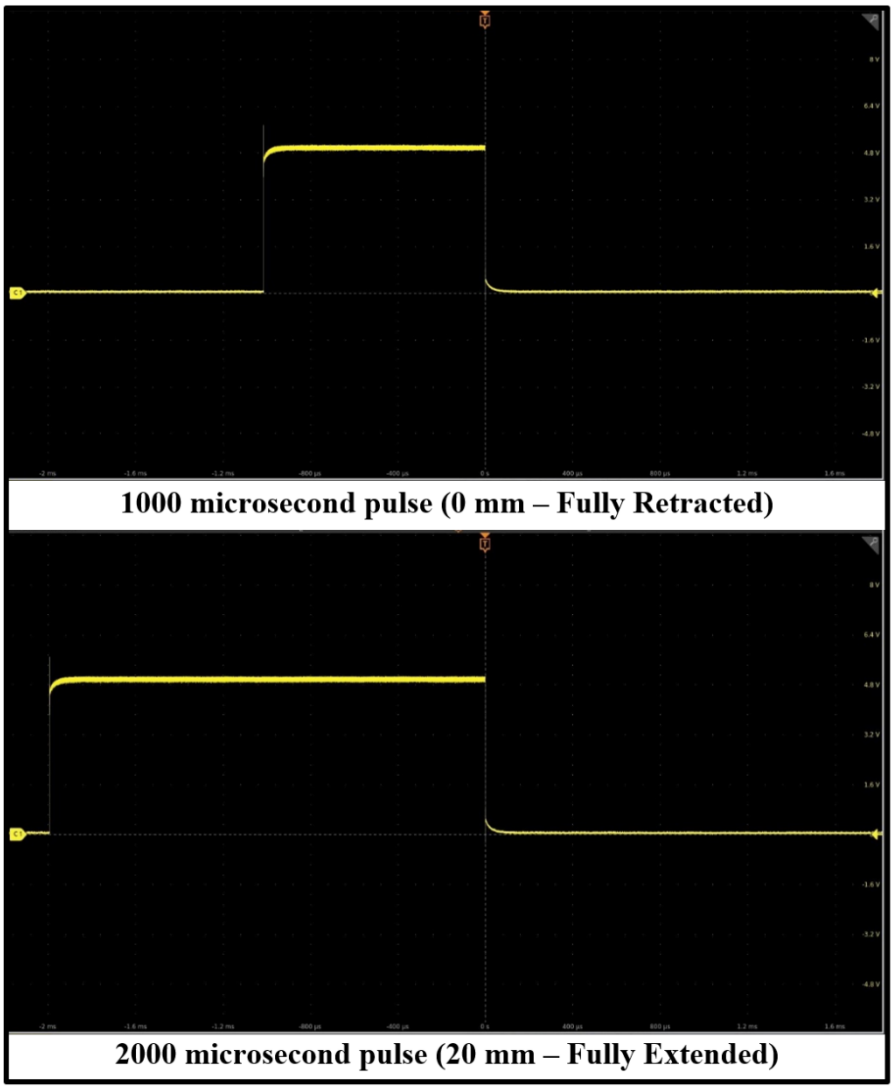

Figure 47. Original Control Signal.

The images illustrate the control signal from the microcontroller when actuator is fully retracted (top) and fully extended (bottom). The actuator was probed with an oscilloscope between the LAC board input and the microcontroller output to obtain readings.

The two images show the original control signal from the microcontroller for the minimum and maximum positions of the servo. The original code utilized the Arduino servo library to provide the control signal. The control signal is a 5V RC hobby servo signal which ranges from 1000-2000 μs at 50 Hz. The LAC board accepts multiple control signals including the signal just described. The board also accepts 0-20 mA or 0-3.3V analog control, USB mini using LabView, and 0-3.3V, 1KHz pulse width modulation, which is what has been employed in the most recent system. Although the hobby servo control signal is a version of pulse width modulation it is not true pulse width modulation [39].

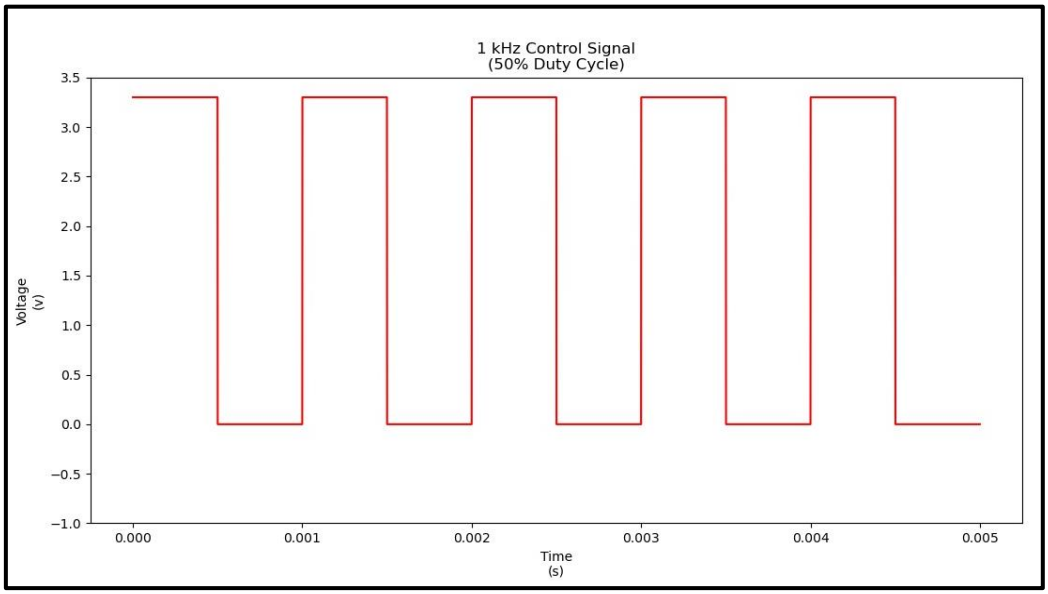

Figure 48. Actuator Control Signal at 1KHz with 50% Duty Cycle.

Plotted output of the expected 0-3.3V 1KHz continuous square wave using Python.

This version works by sending individual pulse at different widths which commands the servo to move to different positions. The 0-3.3V 1KHz PWM is a continuous square wave with a max amplitude of 3.3V and a min amplitude of 0V. The signal oscillates between off and on, the percentage of on time to off time is referred to as

the duty cycle. The servo is adjusted between positions by modulating the duty cycle 0% duty cycle (always off) corresponds to the servo at 0 mm (fully retracted) and 100% duty cycle (always on) corresponds to the servo at 20 mm (fully extended). An example of this signal was emulated using python to simulate what the signal would like on an oscilloscope. The signal shows 5 cycles of the 1KHz 0-3.3V square wave sampled at 10KHz for 0.005 seconds at 50% duty cycle equal times on and off which would command the servo to the 10 mm position (Figure 48). To operate the electrical system, a servo controller code was written using C++. This was completed using the Arduino IDE version 1.8.13. To build the code using the new microcontroller, an Arduino IDE setup for Adafruit QT PY Board was required to flash the code to the microcontroller's flash memory using the built-in bootloader. Once completing this, the code and the circuit board could then communicate through the protocol. Writing the code followed a specific calculation to determine how to program the actuator to perform a displacement that would equate to a desirable strain.

```
/*~~~~~ 5.00-5.50% Strain Cycle ~~~~~*/
  if(states[0] == 1){
  for (i = 0; i < n; i++){
  for (pos = 165; pos >= 100; pos -= 13){
  analogWrite(servoPIN, pos);
  delay(60);
  }
  for (pos = 100; pos <= 165; pos += 13){
  analogWrite(servoPIN, pos);
  delay(60);
  }
   }
    }
```

Figure 49. Operating Code.

The electrical system was directed using this code formatted using Arduino IDE version 1.8.13 to induce 5% strain.

Within the code, adjusting the duty cycle is done by using the "analogWrite" Arduino function. Which has the syntax analogWrite (Pin, 0-255);. The 0-255 values must be whole numbers of the integer type or "int" in C++ (Figure 49). The value of 255 corresponds to 100% duty cycle while 0 corresponds to 0% duty cycle [53]. A calculation was then determined to illustrate the conversion from mm to integers (Figure 50).

$$\frac{Int_{max} - Int_{min}}{Position_{max} - Position_{min}} = \frac{255 - 0}{20mm - 0mm} = 12.75\ \frac{int}{mm} \approx 13\ \frac{int}{mm}\ \because Needs\ whole\ numbers$$

Figure 50. AnalogWrite Arduino Function Calculation.

Due to the length of the shaft, the start position of the servo must be at 13mm, which is approximately 165 as an integer value for the input. The shaft is then adjusted in the code from the start position to various other positions continuously depending on the desired strain. As an example, if the desired cyclic strain is 8% then it is necessary calculate the ideal elongation needed to produce that percentage based on the gauge length of the sample (Figure 51). The gauge length is 33.42mm therefore to find the ideal elongation needed and convert it to an integer. Then to find the input for the end of the range of values subtract the value from the initial position. However, this calculation is an overestimate for the strain because of friction and various reaction forces.

$$165 - (33.42mm)(0.08) * 12.75 \approx 131, \therefore Range\ [131 - 165] \sim 8\%\ \text{continuous cyclic strain}$$

Figure 51. Example Code Calculation to Produce 8% strain.

After testing the code, it was determined that a range of [100-165] produced a strain of 5.0%-5.5%. Using this, it was possible to deviate accordingly and map out a system with the corresponding strain values. Overall, this system is able to operate as a functional electrical system to achieve a desired amount of strain. The system is continuing to be evolved and changed in order to optimize the form of cyclic stretching. Modifications will include reconfiguring the code to achieve a smoother cyclic stretch, as well as quantifying the signal produced by the code output. The final completed bioreactor stretching system was completed using all of the components previously mentioned. (Figure 52) illustrates the bioreactor performing cyclic strain on a PDMS membrane sample. To operate the system, three colored buttons have been installed into the circuit board to give the actuator directions on the amount of strain to apply. Each of these buttons can be programmed using the code and calculation stated before to signify a specific amount of strain. Once pressing a button, an LED light of the same color will turn on to indicate which setting is being performed. An LED control panel display has also been installed to indicate to the user the amount of strain being applied to the substrate for the particular experiment.

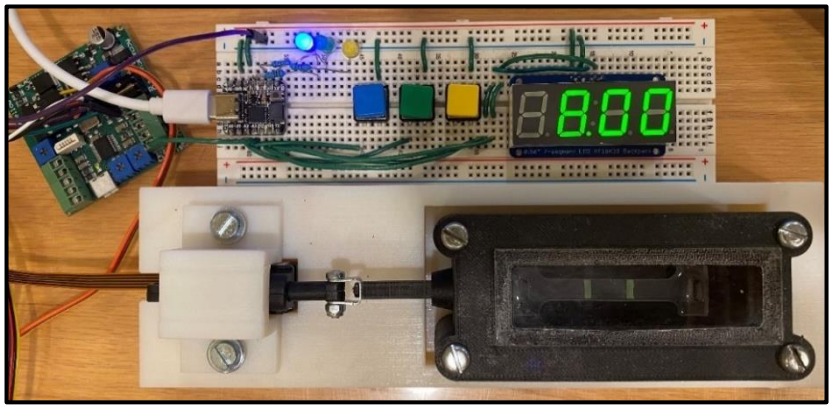

Figure 52. Electrical System.

This system was effective in producing controlled cyclic uniaxial stretching of PDMS.

4.3. Aim 3

This aim illustrated the use of the constructed bioreactor to examine the effect of mechanical loading under reduced gravity conditions using the MC3T3-EI cell-line. These results serve as intriguing preliminary data for future research in this space.

4.3.1. Cell Morphology Results

Visually, the morphology of the cells appeared to vary depending on the treatment group (Figure 53). Cells grown under normal and standard gravity conditions appeared to illustrate traditional cell spreading and morphology as seen with MC3T3-E1 cells. The microgravity and 5% strain groups appeared to be smaller in size and there was a lack of spreading compared to the control. Lastly, the main experimental group illustrating the effect of microgravity and 5% strain illustrated the most abnormal morphology and a lack of spreading.

To further quantify the morphology of the cells, the cell area was measured and calculated using ImageJ. The data was compiled for each of the groups and were statistically analyzed using an ANOVA one way variance analysis. The analysis was conducted using an alpha of 0.05 with a confidence level of 95%. The data was graphically represented using a boxplot with the error bars referring to the range and interquartile range. The analysis indicated that there were highly significant differences comparing the cell area of the cytoskeleton amongst the different treatment groups (Figure 54).

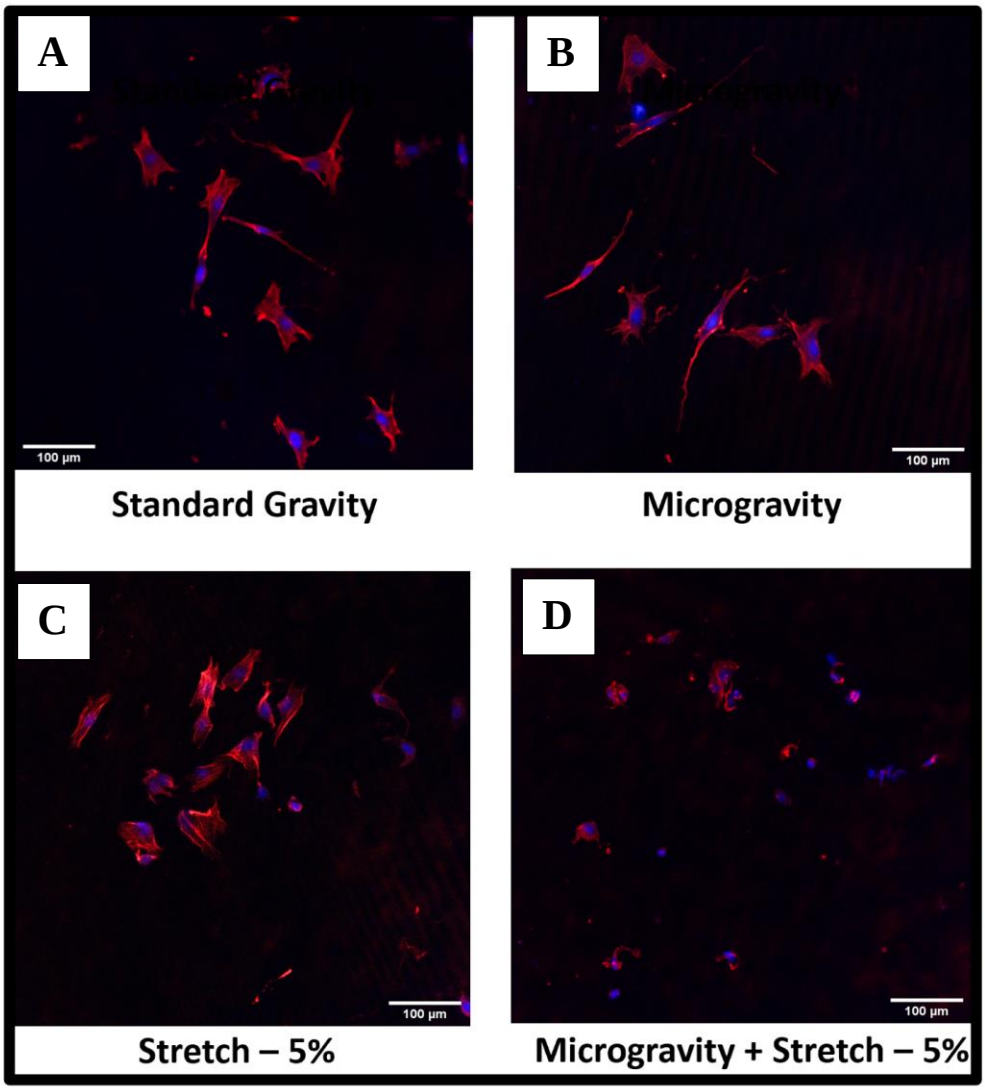

Figure 53. Cell Morphology of MC3T3-E1 Cells.

Cells were stained with Hoechst (Blue) and Phalloidin (red). (A) Standard Gravity, (B) Microgravity, (C) Stretch at 5% strain, and (D) Microgravity and 5% strain.

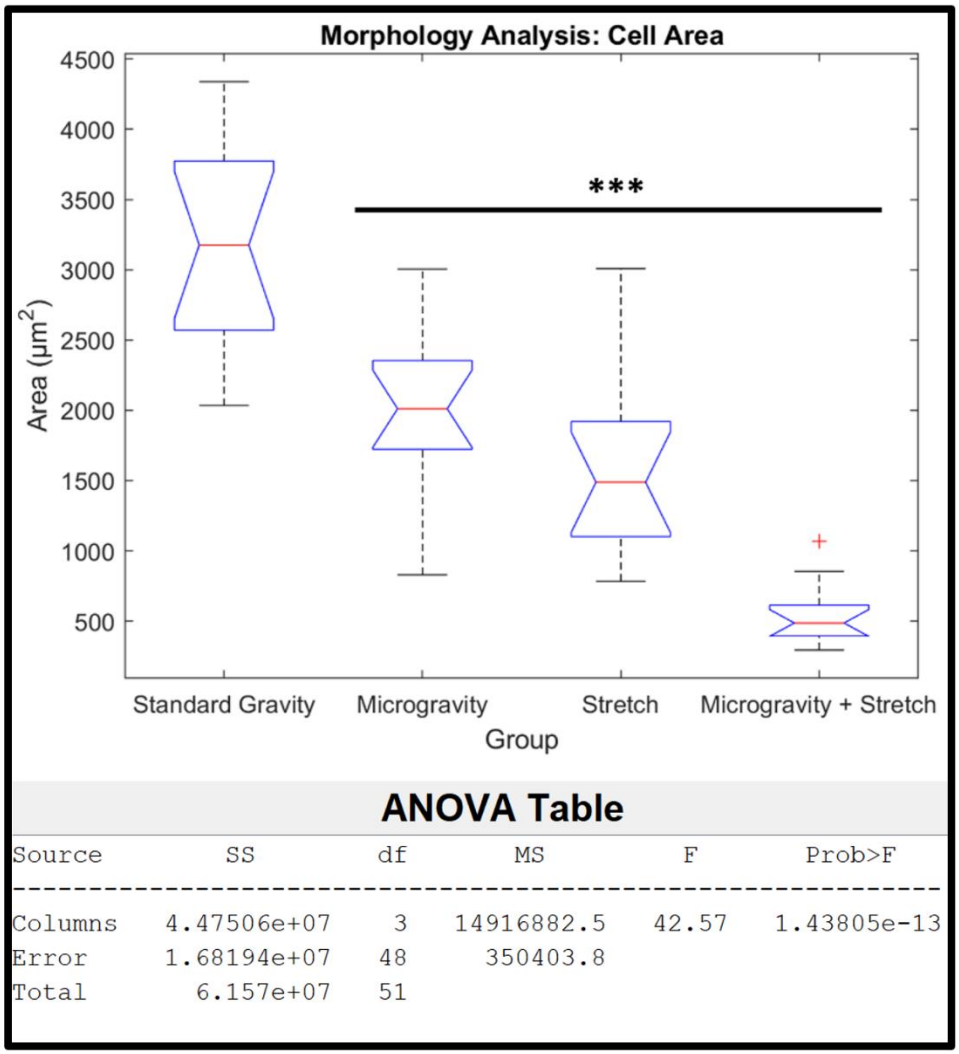

ANOVA Table

Source	SS	df	MS	F	Prob>F
Columns	4.47506e+07	3	14916882.5	42.57	1.43805e-13
Error	1.68194e+07	48	350403.8		
Total	6.157e+07	51			

Figure 54. ANOVA one-way Analysis of Cytoskeleton Area.

Cell Morphology comparing the different treatment groups in regard to cell area of the cytoskeleton. The results indicated a p-value of < 0.001 which corresponds to there being significant statistical differences between the groups. Error bars correspond to the range and interquartile range.

Another ANOVA analysis was conducted to compare the two treatment groups of microgravity and 5% strain (Figure 55). When comparing the cells in these groups, there were no statistical differences found when comparing the cell area.

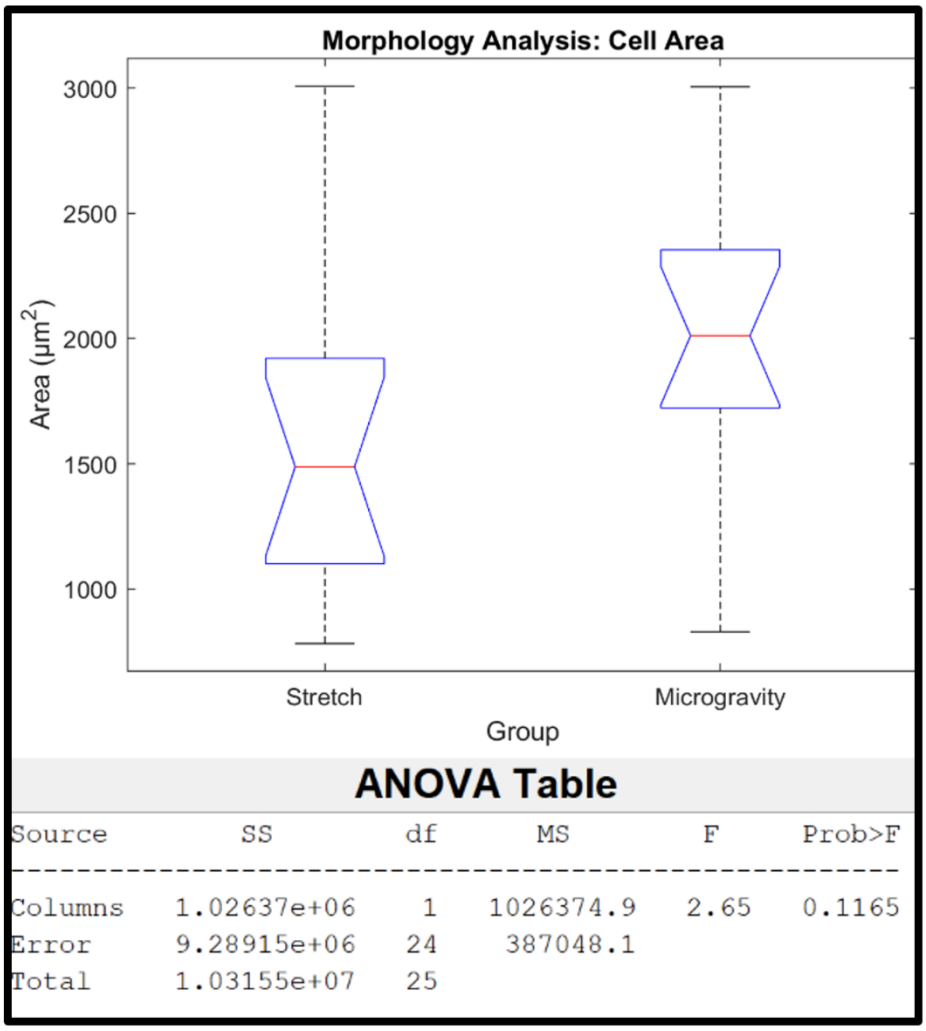

ANOVA Table

Source	SS	df	MS	F	Prob>F
Columns	1.02637e+06	1	1026374.9	2.65	0.1165
Error	9.28915e+06	24	387048.1		
Total	1.03155e+07	25			

Figure 55. ANOVA One-way Analysis of Cell Morphology.

This analysis compared the 5% stretch and microgravity groups in regard to cell area of the cytoskeleton. The results indicated a p-value of 0.1165, which corresponds to ns differences between the groups. Error bars correspond to the range and interquartile range.

The cell area of the nuclei was also measured and compared using an ANOVA one-way analysis for each of the groups (Figure 56). The results illustrated a p-value of <0.001 which indicates that there are statistical differences between groups in regard to the cell area of the nuclei.

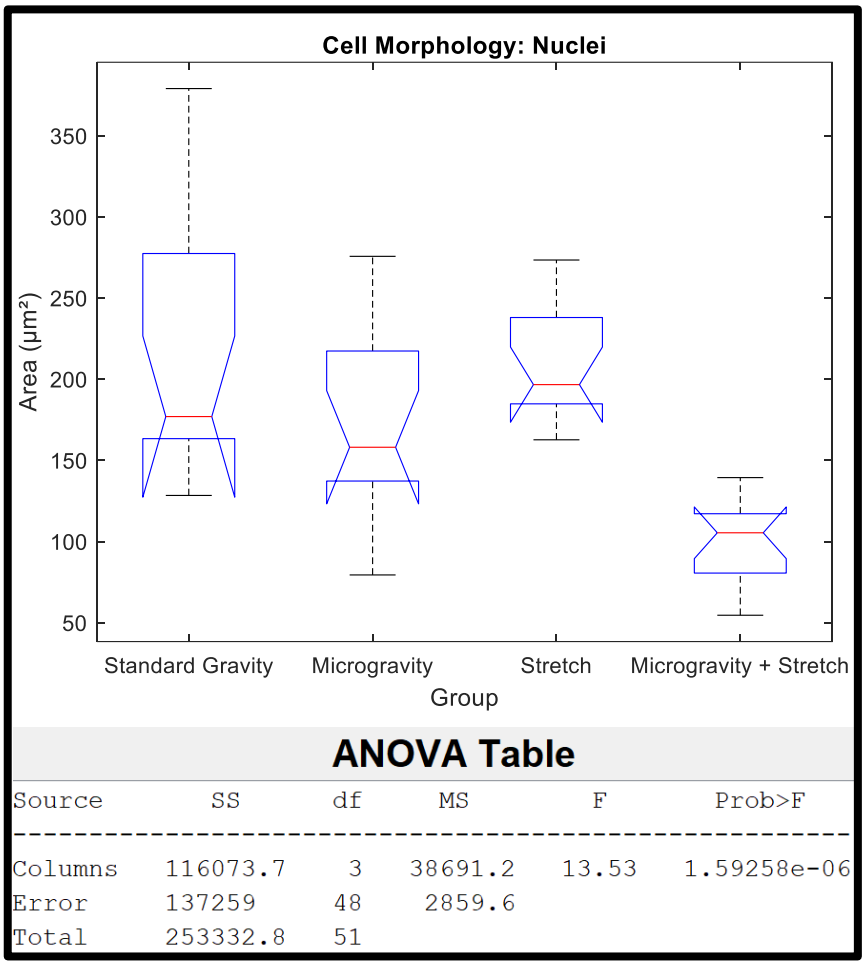

ANOVA Table

Source	SS	df	MS	F	Prob>F
Columns	116073.7	3	38691.2	13.53	1.59258e-06
Error	137259	48	2859.6		
Total	253332.8	51			

Figure 56: ANOVA One-way Analysis of Nuclei Area.

Cell Morphology comparing the 5% stretch and microgravity groups in regard to cell area of the nuclei. The results indicated a p-value of <0.001, which corresponds to significant statistical differences between the groups. Error bars correspond to the range and interquartile range.

Looking at the results, the experimental group of microgravity and 5% stretch illustrated the smallest nuclei area compared to the others. This statistical analysis was conducted again using ANOVA to determine if there was a statistical difference in nuclei area comparing the groups of standard gravity, microgravity and 5% stretch (Figure 57). The results illustrated that there were no statistical differences in nuclei area when only comparing these groups, according to the p-value of 0.0909.

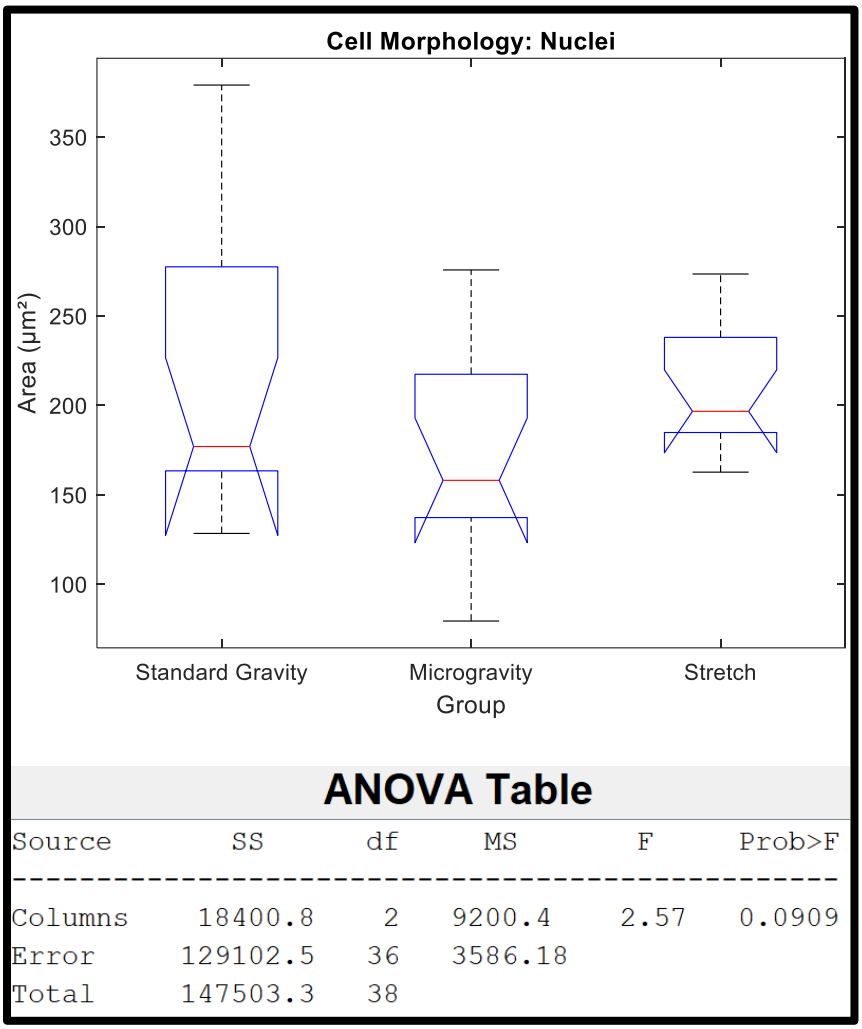

ANOVA Table

Source	SS	df	MS	F	Prob>F
Columns	18400.8	2	9200.4	2.57	0.0909
Error	129102.5	36	3586.18		
Total	147503.3	38			

Figure 57. ANOVA One-way Analysis of Cell Morphology.

ANOVA comparison between the standard gravity, microgravity, and 5% stretch groups in regard to cell area of the nuclei. The results indicated a p-value of 0.0909, which corresponds to no statistical differences between the groups. Error bars correspond to the range and interquartile range.

Overall, these findings were able to provide preliminary research and data using the fabricated microgravity stretch bioreactor. More data must be retrieved in order to determine the validity of the results expressed. With the collection of more data from increased experimentation, additional analyses can be conducted including cell alignment

to determine the orientation of strain, shape elongation factor of the nuclei, and the effect of varying strain/gravitational conditions. These analyses were unable to be conducted to an insufficient quantity and quality of data and also because of the usage demand for the RPM, which caused time constraints.

CHAPTER 5

5. DISCUSSION

The purpose of this project is to provide a means to research the effect of applied strain on osteoblasts in partial or microgravity environments in order to determine if mechanical loading can reduce the deleterious effects of a 0G environment. Devices have been created to experiment how each of these factors affect cellular development independently, yet there is no device that is able to apply strain to cells while subjected to reduced gravitational conditions simultaneously. The formulation of such a device is of great importance since it can be used as a tool to study the effect of long-term space flight. Astronauts who have gone on extended spaceflights must constantly perform exercises while in space that will induce mechanical stress and strain on their skeletal tissue in order to compensate for the lack of mechanical loading due to the absence of gravity. For these reasons, the ability to construct a bioreactor that is able to induce the effect of mechanical loading on cells while under microgravity conditions can be utilized to better understand the effects of space travel on the human biological make-up.

5.1. PDMS Membrane Development

The first major area of the project was to develop a PDMS membrane that could be used as a suitable substrate for uniaxial cyclic stretching of cells. This was completed by creating an innovative membrane design that would allow for uniform strain across the membrane during stretch. The mechanical properties of the formulated membrane were evaluated using mathematical modelling, tensile testing, fatigue testing, and through the use of a strain characterization analysis. The results indicated that the design and formulation of the PDMS membrane are appropriate for such a strain device within the relevant biological limit used for bone cells.

5.2. Bioreactor Development

The goal of this project was to develop a bioreactor capable of applying cyclic uniaxial strain on cells while under reduced gravitational conditions. In doing so, a novel bioreactor device was designed and constructed using a variety of custom-made 3D printed parts. The device and its components were validated and tested using actuator performance testing, biocompatibility testing, and gas permeability assays. The results indicated that such a device was suitable for cellular stretching conditions and that the bioreactor is able to fully work in conjunction with a Random Positioning Machine.

5.3. Cell Morphology Experimentation

The constructed bioreactor was used to run cell morphological experimentation using osteoblasts cultured under various conditions. The set-up of the device allows for microgravity and strain under microgravity conditions to be examined concurrently. Cells were evaluated under the different conditions using the device and were compared in regard to cell area. The results indicated that there was an effect in the overall cell size and spreading using the designed bioreactor compared to the control. Overall, these preliminary studies allow for future experimentation using the device.

5.4. Conclusions

Overall, the results and findings were able to provide for preliminary data using the constructed bioreactor device. This fully functional device is able to apply uniaxial strain to cells while subjected to reduced gravity conditions presented by a Random Positioning Machine. The ability to use such a device in conjunction with the RPM is truly unique in its design and development and this system can be used as a valuable research tool in the future. The next steps for such research would be to examine how each of the treatments affect osteogenic differentiation through the means of an alkaline phosphatase activity

assay. Unfortunately, because of time limitations due to high usage demand for the RPM, this experimentation was not completed. The ability to use this device can ultimately allow for many different types of experimentation and this research will be examined for future and ongoing studies.

REFERENCES CITED

[1] B. R. Unsworth and P. I. Lelkes, "Growing tissues in microgravity," *Nat. Med.,* vol. 4, *(8),* pp. 901-907, 1998. Available: https://doi.org/10.1038/nm0898-901. DOI: 10.1038/nm0898-901.

[2] D. Grimm *et al*, "Growing tissues in real and simulated microgravity: new methods for tissue engineering," *Tissue Engineering.Part B, Reviews,* vol. 20, *(6),* pp. 555-566, 2014. Available: https://pubmed.ncbi.nlm.nih.gov/24597549 https://www.ncbi.nlm.nih.gov/pmc/articles/PMC4241976/. DOI: 10.1089/ten.TEB.2013.0704.

[3] R. Florencio-Silva *et al*, "Biology of Bone Tissue: Structure, Function, and Factors That Influence Bone Cells," *BioMed Research International,* vol. 2015, pp. 421746, 2015. Available: https://pubmed.ncbi.nlm.nih.gov/26247020 https://www.ncbi.nlm.nih.gov/pmc/articles/PMC4515490/. DOI: 10.1155/2015/421746.

[4] A. M. Mohamed, "An overview of bone cells and their regulating factors of differentiation," *The Malaysian Journal of Medical Sciences : MJMS,* vol. 15, *(1),* pp. 4-12, 2008. Available: https://pubmed.ncbi.nlm.nih.gov/22589609 https://www.ncbi.nlm.nih.gov/pmc/articles/PMC3341892/.

[5] A. Lomri and P. J. Marie, "The cytoskeleton in the biology of bone cells," *The Cytoskeleton: A Multi-Volume Treatise,* vol. 3, pp. 229-263, 1996. Available: https://www-sciencedirect-com.libproxy.temple.edu/science/article/pii/S1874602096800103. DOI: https://doi-org.libproxy.temple.edu/10.1016/S1874-6020(96)80010-3.

[6] M. T. Valenti, L. Dalle Carbonare and M. Mottes, "Osteogenic Differentiation in Healthy and Pathological Conditions," *International Journal of Molecular Sciences,* vol. 18, *(1),* pp. 41, 2016. Available: https://pubmed.ncbi.nlm.nih.gov/28035992 https://www.ncbi.nlm.nih.gov/pmc/articles/PMC5297676/. DOI: 10.3390/ijms18010041.

[7] N. Nabavi *et al*, "Effects of microgravity on osteoclast bone resorption and osteoblast cytoskeletal organization and adhesion," *Bone,* vol. 49, *(5),* pp. 965-974, 2011. Available: https://www-sciencedirect-com.libproxy.temple.edu/science/article/pii/S8756328211011380. DOI: https://doi-org.libproxy.temple.edu/10.1016/j.bone.2011.07.036.

[8] D. Grimm *et al*, "The impact of microgravity on bone in humans," *Bone,* vol. 87, pp. 44-56, 2016. Available: https://www.sciencedirect.com/science/article/pii/S8756328216300783. DOI: https://doi.org/10.1016/j.bone.2015.12.057.

[9] J. P. R. Scott, T. Weber and D. A. Green, "Introduction to the Frontiers Research Topic: Optimization of Exercise Countermeasures for Human Space Flight - Lessons From Terrestrial Physiology and Operational Considerations," *Frontiers in Physiology,* vol. 10, pp. 173, 2019. Available: https://pubmed.ncbi.nlm.nih.gov/30899226 https://www.ncbi.nlm.nih.gov/pmc/articles/PMC6416179/. DOI: 10.3389/fphys.2019.00173.

[10] W. Shi *et al*, "Microgravity induces inhibition of osteoblastic differentiation and mineralization through abrogating primary cilia," *Scientific Reports,* vol. 7, *(1),* pp. 1866, 2017. Available: https://pubmed.ncbi.nlm.nih.gov/28500304 https://www.ncbi.nlm.nih.gov/pmc/articles/PMC5431935/. DOI: 10.1038/s41598-017-02049-9.

[11] T. Hoson *et al*, "Evaluation of the three-dimensional clinostat as a simulator of weightlessness," *Planta,* vol. 203, *(1),* pp. S187-S197, 1997. Available: https://doi.org/10.1007/PL00008108. DOI: 10.1007/PL00008108.

[12] C. Ulbrich *et al*, "The impact of simulated and real microgravity on bone cells and mesenchymal stem cells," *BioMed Research International,* vol. 2014, pp. 928507, 2014. Available: https://pubmed.ncbi.nlm.nih.gov/25110709 https://www.ncbi.nlm.nih.gov/pmc/articles/PMC4119729/. DOI: 10.1155/2014/928507.

[13] C. Neidlinger-Wilke *et al*, "Cell alignment is induced by cyclic changes in cell length: studies of cells grown in cyclically stretched substrates," *Journal of Orthopaedic Research,* vol. 19, *(2),* pp. 286-293, 2001. Available: https://www.sciencedirect.com/science/article/pii/S0736026600000292. DOI: https://doi.org/10.1016/S0736-0266(00)00029-2.

[14] T. Hammond and P. Allen, "The Bonn Criteria: Minimal Experimental Parameter Reporting for Clinostat and Random Positioning Machine Experiments with Cells and Tissues," *Microgravity Sci Technol,* vol. 23, *(2),* pp. 271-275, 2011. Available: https://doi.org/10.1007/s12217-010-9226-5. DOI: 10.1007/s12217-010-9226-5.

[15] C. A. D. Leguy *et al*, "Fluid motion for microgravity simulations in a random positioning machine," *Gravitational and Space Biology,* vol. 25, pp. 36+, 2011. Available: https://link-gale-com.libproxy.temple.edu/apps/doc/A348311321/AONE?u=temple_main&sid=AONE&xid=a94978ff.

[16] A. G. Borst and van Loon, Jack J. W. A., "Technology and Developments for the Random Positioning Machine, RPM," *Microgravity Sci Technol,* vol. 21, *(4),* pp. 287, 2008. Available: https://doi.org/10.1007/s12217-008-9043-2. DOI: 10.1007/s12217-008-9043-2.

[17] B. D. Hoffman, C. Grashoff and M. A. Schwartz, "Dynamic molecular processes mediate cellular mechanotransduction," *Nature,* vol. 475, *(7356),* pp. 316-323, 2011. Available: https://pubmed.ncbi.nlm.nih.gov/21776077 https://www.ncbi.nlm.nih.gov/pmc/articles/PMC6449687/. DOI: 10.1038/nature10316.

[18] A. W. Orr *et al*, "Mechanisms of Mechanotransduction," *Developmental Cell,* vol. 10, *(1),* pp. 11-20, 2006. Available: https://www.sciencedirect.com/science/article/pii/S153458070500482X. DOI: https://doi.org/10.1016/j.devcel.2005.12.006.

[19] Y. Mikuni-Takagaki *et al*, "Distinct responses of different populations of bone cells to mechanical stress," *Endocrinology,* vol. 137, *(5),* pp. 2028-2035, 1996. Available: https://doi.org/10.1210/endo.137.5.8612544. DOI: 10.1210/endo.137.5.8612544.

[20] H. Atcha *et al*, "A Low-Cost Mechanical Stretching Device for Uniaxial Strain of Cells: A Platform for Pedagogy in Mechanobiology," *J. Biomech. Eng.,* vol. 140, *(8),* pp. 810051, 2018. Available: https://pubmed.ncbi.nlm.nih.gov/30003248 https://www.ncbi.nlm.nih.gov/pmc/articles/PMC6056193/. DOI: 10.1115/1.4039949.

[21] J. Kreutzer *et al*, "Pneumatic cell stretching system for cardiac differentiation and culture," *Med. Eng. Phys.,* vol. 36, *(4),* pp. 496-501, 2014. Available: https://www.sciencedirect.com/science/article/pii/S1350453313002178. DOI: https://doi.org/10.1016/j.medengphy.2013.09.008.

[22] K. Shimizu *et al*, "Development of a biochip with serially connected pneumatic balloons for cell-stretching culture," *Sensors Actuators B: Chem.,* vol. 156, *(1),* pp. 486-493, 2011. Available: https://www.sciencedirect.com/science/article/pii/S0925400511003455. DOI: https://doi.org/10.1016/j.snb.2011.04.048.

[23] K. Harshad *et al*, "An electromagnetic cell-stretching device for mechanotransduction studies of olfactory ensheathing cells," *Biomed. Microdevices,* vol. 18, *(3),* pp. 45, 2016. Available: https://doi.org/10.1007/s10544-016-0071-1. DOI: 10.1007/s10544-016-0071-1.

[24] C. Frias *et al*, "Piezoelectric actuator: Searching inspiration in nature for osteoblast stimulation," *Composites Sci. Technol.,* vol. 70, *(13),* pp. 1920-1925, 2010. Available: https://www.sciencedirect.com/science/article/pii/S026635381000237X. DOI: https://doi.org/10.1016/j.compscitech.2010.06.011.

[25] S. P. Arold, J. Y. Wong and B. Suki, "Design of a New Stretching Apparatus and the Effects of Cyclic Strain and Substratum on Mouse Lung Epithelial-12 Cells," *Ann. Biomed. Eng.*, vol. 35, *(7)*, pp. 1156-64, 2007. Available: http://libproxy.temple.edu/login?url=https://www-proquest-com.libproxy.temple.edu/scholarly-journals/design-new-stretching-apparatus-effects-cyclic/docview/756671768/se-2?accountid=14270. DOI: http://dx.doi.org.libproxy.temple.edu/10.1007/s10439-007-9262-5.

[26] M. J. Buckley, A. J. Banes and R. D. Jordan, "The effects of mechanical strain on osteoblasts in vitro," *Journal of Oral and Maxillofacial Surgery*, vol. 48, *(3)*, pp. 276-282, 1990. Available: https://www.sciencedirect.com/science/article/pii/027823919090393G. DOI: https://doi.org/10.1016/0278-2391(90)90393-G.

[27] L. Tang, Z. Lin and Y. Li, "Effects of different magnitudes of mechanical strain on Osteoblasts in vitro," *Biochem. Biophys. Res. Commun.*, vol. 344, *(1)*, pp. 122-128, 2006. Available: https://www.sciencedirect.com/science/article/pii/S0006291X06006760. DOI: https://doi.org/10.1016/j.bbrc.2006.03.123.

[28] J. N. Lee *et al*, "Compatibility of Mammalian Cells on Surfaces of Poly(dimethylsiloxane)," *Langmuir*, vol. 20, *(26)*, pp. 11684-11691, 2004. Available: https://doi.org/10.1021/la048562+. DOI: 10.1021/la048562+.

[29] I. D. Johnston *et al*, "Mechanical characterization of bulk Sylgard 184 for microfluidics and microengineering," *Jmm*, vol. 24, *(3)*, 2014. Available: https://iopscience.iop.org/article/10.1088/0960-1317/24/3/035017. DOI: 10.1088/0960-1317/24/3/035017.

[30] Z. Wang *et al*, "Stretchable materials of high toughness and low hysteresis," *Proc. Natl. Acad. Sci. U. S. A.*, vol. 116, *(13)*, pp. 5967-5972, 2019. Available: https://pubmed.ncbi.nlm.nih.gov/30850517 https://www.ncbi.nlm.nih.gov/pmc/articles/PMC6442615/. DOI: 10.1073/pnas.1821420116.

[31] A. Mata, A. J. Fleischman and S. Roy, "Characterization of Polydimethylsiloxane (PDMS) Properties for Biomedical Micro/Nanosystems," *Biomed. Microdevices*, vol. 7, *(4)*, pp. 281-293, 2005. Available: https://doi.org/10.1007/s10544-005-6070-2. DOI: 10.1007/s10544-005-6070-2.

[32] Z. Wang, A. A. Volinsky and N. D. Gallant, "Crosslinking effect on polydimethylsiloxane elastic modulus measured by custom-built compression instrument," *J Appl Polym Sci*, vol. 131, *(22)*, 2014. Available: https://doi.org/10.1002/app.41050. DOI: https://doi.org/10.1002/app.41050.

[33] Markforged, "Material datasheet composites," 2020.

[34] E. Boulter *et al*, "Cyclic uniaxial mechanical stretching of cells using a LEGO® parts-based mechanical stretcher system," *J. Cell. Sci.*, vol. 133, *(1)*, pp. jcs234666, 2020. Available: http://jcs.biologists.org/content/133/1/jcs234666.abstract. DOI: 10.1242/jcs.234666.

[35] T. S. Lumpe, J. Mueller and K. Shea, "Tensile properties of multi-material interfaces in 3D printed parts," *Mater Des*, vol. 162, pp. 1-9, 2019. Available: https://www.sciencedirect.com/science/article/pii/S0264127518308311. DOI: https://doi.org/10.1016/j.matdes.2018.11.024.

[36] M. Xu, D. J. McCanna and J. G. Sivak, "Use of the viability reagent PrestoBlue in comparison with alamarBlue and MTT to assess the viability of human corneal epithelial cells," *J. Pharmacol. Toxicol. Methods*, vol. 71, pp. 1-7, 2015. Available: https://www.sciencedirect.com/science/article/pii/S1056871914002809. DOI: https://doi.org/10.1016/j.vascn.2014.11.003.

[37] S. N. Rampersad, "Multiple applications of Alamar Blue as an indicator of metabolic function and cellular health in cell viability bioassays," *Sensors (Basel, Switzerland)*, vol. 12, *(9)*, pp. 12347-12360, 2012. Available: https://pubmed.ncbi.nlm.nih.gov/23112716 https://www.ncbi.nlm.nih.gov/pmc/articles/PMC3478843/. DOI: 10.3390/s120912347.

[38] Actuonix Motion Devices Inc., "Miniature linear motion series PQ12," 2019.

[39] Actuonix Motion Devices Inc., "LAC actuonix linear actuator control board," 2018.

[40] Arduino, "Arduino uno Rev3," 2021.

[41] K. Rembor, "Adafruit QT py overview," 2015.

[42] A. Guignandon *et al*, "Cyclic strain promotes shuttling of PYK2/Hic-5 complex from focal contacts in osteoblast-like cells," *Biochem. Biophys. Res. Commun.*, vol. 343, *(2)*, pp. 407-414, 2006. Available: https://www.sciencedirect.com/science/article/pii/S0006291X06004347. DOI: https://doi.org/10.1016/j.bbrc.2006.02.162.

[43] S. Hasegawa *et al*, "Mechanical stretching increases the number of cultured bone cells synthesizing DNA and alters their pattern of protein synthesis," *Calcif. Tissue Int.*, vol. 37, *(4)*, pp. 431-436, 1985. Available: https://doi.org/10.1007/BF02553714. DOI: 10.1007/BF02553714.

[44] H. Yu *et al*, "Impact of mechanical stretch on the cell behaviors of bone and surrounding tissues," *Journal of Tissue Engineering*, vol. 7, pp. 2041731415618342, 2016. Available: https://pubmed.ncbi.nlm.nih.gov/26977284 https://www.ncbi.nlm.nih.gov/pmc/articles/PMC4765821/. DOI: 10.1177/2041731415618342.

[45] M. Gencheva *et al*, "Bone marrow osteoblast vulnerability to chemotherapy," *Eur. J. Haematol.*, vol. 90, *(6)*, pp. 469-478, 2013. Available: https://pubmed.ncbi.nlm.nih.gov/23551534 https://www.ncbi.nlm.nih.gov/pmc/articles/PMC3662303/. DOI: 10.1111/ejh.12109.

[46] P. Wipff *et al*, "The covalent attachment of adhesion molecules to silicone membranes for cell stretching applications," *Biomaterials*, vol. 30, *(9)*, pp. 1781-1789, 2009. Available: https://www.sciencedirect.com/science/article/pii/S0142961208009873. DOI: https://doi.org/10.1016/j.biomaterials.2008.12.022.

[47] E. Jastrzebska *et al*, "Biological characterization of the modified poly(dimethylsiloxane) surfaces based on cell attachment and toxicity assays," *Biomicrofluidics*, vol. 12, *(4)*, pp. 044105, 2018. Available: https://pubmed.ncbi.nlm.nih.gov/30034568 https://www.ncbi.nlm.nih.gov/pmc/articles/PMC6039296/. DOI: 10.1063/1.5035176.

[48] K. Anselme, "Osteoblast adhesion on biomaterials," *Biomaterials*, vol. 21, 2000.

[49] A. Zuchowska *et al*, "Adhesion of MRC-5 and A549 cells on poly(dimethylsiloxane) surface modified by proteins," *Electrophoresis*, vol. 37, *(3)*, pp. 536-544, 2016. Available: https://doi.org/10.1002/elps.201500250. DOI: https://doi.org/10.1002/elps.201500250.

[50] Z. Li *et al*, "Uniaxial Static Strain Promotes Osteoblast Proliferation and Bone Matrix Formation in Distraction Osteogenesis In Vitro," *BioMed Research International*, vol. 2020, pp. 3906426, 2020. Available: https://doi.org/10.1155/2020/3906426. DOI: 10.1155/2020/3906426.

[51] A. S. Cruz-Félix *et al*, "PDMS samples characterization with variations of synthesis parameters for tunable optics applications," *Heliyon*, vol. 5, *(12)*, pp. e03064, 2019. Available: https://www.sciencedirect.com/science/article/pii/S2405844019367234. DOI: https://doi.org/10.1016/j.heliyon.2019.e03064.

[52] A. Souza *et al*, "Characterization of Shear Strain on PDMS: Numerical and Experimental Approaches," *Applied Sciences*, vol. 10, *(9)*, 2020. . DOI: 10.3390/app10093322.

[53] Arduino, "PWM project hub," 2016.